Applied Surface Science 389 (2016) 651–665

Contents lists available at ScienceDirect

Applied Surface Science

journal homepage: www.elsevier.com/locate/apsusc

PEEK (polyether-ether-ketone)-coated nitinol wire: Film stability for biocompatibility applications

Nataliia Sheiko[a], Patrick Kékicheff[a,*], Pascal Marie[a], Marc Schmutz[a], Leandro Jacomine[a], Fabienne Perrin-Schmitt[b]

[a] Institut Charles Sadron, C.N.R.S. UPR 22, Université de Strasbourg, 23 rue du Loess, BP 84047, 67034 Strasbourg Cedex 2, France
[b] Faculté de Médecine, INSERM, UMR-S 1121, "Biomaterials and Bioengineering", Université de Strasbourg, 11 rue Humann, 67085 Strasbourg Cedex, France

ARTICLE INFO

Article history:
Received 1 July 2016
Received in revised form 25 July 2016
Accepted 27 July 2016
Available online 29 July 2016

Keywords:
Biomaterials
TiNi alloy
Biocompatibility
coating
PEEK
Nanoscratch

ABSTRACT

High quality biocompatible poly-ether-ether-ketone (PEEK) coatings were produced on NiTi shape memory alloy wires using dipping deposition from colloidal aqueous PEEK dispersions after substrate surface treatment. The surface morphology and microstructure were investigated by Scanning Electron Microscopy at every step of the process from the as-received Nitinol substrate to the ultimate PEEK-coated NiTi wire. Nanoscratch tests were carried out to access the adhesive behavior of the polymer coated film to the NiTi. The results indicate that the optimum process conditions in cleaning, chemical etching, and electropolishing the NiTi, were the most important and determining parameters to be achieved. Thus, high quality PEEK coatings were obtained on NiTi wires, straight or curved (even with a U-shape) with a homogeneous microstructure along the wire length and a uniform thickness of 12 μm without any development of cracks or the presence of large voids. The biocompatibility of the PEEK coating film was checked in fibrobast cultured cells. The coating remains stable in biological environment with negligible Ni ion release, no cytotoxicity, and no delamination observed with time.

1. Introduction

Advanced thermoplastic materials such as polyaromatic semicrystalline poly-ether-ether-ketone (PEEK) are used increasingly for many industrial applications [1]. Beyond advantages of enhanced mechanical properties combined with high thermal and chemical stability allowing high-performance applications to be performed in chemical processing, aerospace, and automative, PEEK is appealing for medical industries following confirmation of its biocompatibility three decades ago [2]. Its superior combination of strength, stiffness and toughness confirms its suitability for in vivo medical device instruments and implants with applications in orthopaedics and trauma medicine, including fracture fixation plates, osteosynthesis plates, screws, intramedullary nails, external fixators or finger-joint prostheses [3–6]. As PEEK polymer is non-cytotoxic it can be repeatedly sterilized using conventional steam, gamma and ethylene oxide processes without evident deterioration of its mechanical properties [1].

However, despite its outstanding chemical and hydrolysis resistance, high strength and excellent tribological properties with extensive biocompatibility for use in orthopaedics, cardiopulmonary and dental areas, PEEK is still a relatively mechanically weak material in its homogeneous form. Therefore an ideal combination has been sought for the last decade where PEEK could be applied as a coating on a strong material. In particular, combining the outstanding properties of PEEK as a coating biocompatible film with the ones of nickel-titanium shape memory alloys as a substrate is appealing.

Indeed, these alloys possess unique properties like the thermal shape memory, superelasticity and good damping, due to a reversible solid-solid phase transformation between a high symmetry austenitic crystal structure and a lower symmetry martensitic structure. Since the 1970′s they have been introduced to medical applications progressively replacing medical devices manufactured with other materials (stainless steel, alloys, Co—Cr—Mo) [7]. NiTi alloy was named "nickel titanium" or Nitinol® from its constituents (Nickel and Titanium present in roughly equal atomic percentages) and the name of the place where it was designed — the Nickel Titanium Naval Ordnance Laboratory (NOL, Maryland, USA). Thanks to their good resistance to corrosion and high biocompatibility [8,9] NiTi alloys are currently used

* Corresponding author.
E-mail address: patrick.kekicheff@ics-cnrs.unistra.fr (P. Kékicheff).

http://dx.doi.org/10.1016/j.apsusc.2016.07.159
0169-4332/

as "smart" devices of small size that can be incorporated into various structures of the human body with minimal damage. When applied in certain surgical implants NiTi provides a possibility to make self-locking, self-expanding and self-compressing implants activating at body temperature [10]. Therefore they have been used as intravascular implants and filters, vascular, urethral and biliary stents, valves, bone and dental implants, orthodontic wires for manufacturing arc, extractors biliary and urinary stones catheters, clips, clamps, surgical instruments, etc. [1,7–13].

The other advantage of coating NiTi alloys by a biocompatible film reduces and ultimately eliminates the risk of any material corrosion. Indeed, the high content of nickel Ni (45–55%) in the alloy causes some concern for potential users, since the release of nickel atoms from the surface of the implant and their eventual accumulation above a critical concentration threshold may yield to an allergic response in the body and induce toxic effects [8,9,12,14,15]. Because the diameter of Nitinol wire in use can be extremely small, ranging from few millimeters to 20 μm, the corrosion standards developed for large articles or implants may be not satisfactory in the case of medical devices utilizing thin Nitinol wires. Even if several studies [16–18] have shown that such fears do not have serious grounds because high nickel content in the alloy does not necessarily mean a high degree of release of these atoms from the surface, the medical industry prefers to fully eliminate the possibility of material corrosion when long-term contact with living tissues is sought [19] since corrosion marks were noted in different reports such as those found for Nitinol arch wires after 1–6 months in the mouth [20] or for Nitinol endografts explanted after 13–53 months [21] to name just a few.

Thus to create an effective barrier to Ni ion diffusion from the NiTi alloy is to cover its surface with organic or inorganic coatings and in such way combine the extraordinary mechanical properties of NiTi with biocompatible properties of non-metallic coatings [22–29]. Nowadays several methods of covering have been developed, including ion-beam sputtering, chemical vapor deposition, sol-gel coatings, electrophoresis, electrochemical deposition, thermal and plasma spraying, enameling, etc. [30–32]. Varying degrees of success have been achieved because mechanical or thermal stresses are involved in the processes. Furthermore the common problem encountered with coatings for Nitinol is that their adhesion is worsened inevitably because of the alteration in surface topography associated with formation of a relief when phase transformation to martensite is induced. As a consequence the mechanical interlocking often considered as the primary adhesion mechanism between coating and substrate [32] is not always sufficient: despite the fact that adhesion can usually be improved by grit-blasting substrate before film deposition, the use of surface texturing to modify and control the wetting of foundry materials and brazements has been shown to reach some limits [33,34]. Indeed an increase in surface roughness, to some extent, can lead to a reduction of wettability of the material particles due to barrier formations, such as peaks, ridges and asperities [32–34].

These reported drawbacks have invited us to follow the opposite approach for polymer coating on Nitinol. In this interesting direction to explore because polymer elasticity is compatible with that of Nitinol, we appropriately prepared the Nitinol surface before coating deposition, with a reduced and controlled roughness and the best possible surface homogeneity following our patented procedure [35]. We illustrate our method by coating Nitinol wires with a polyether-ether-ketone (PEEK) thin film (about 12 μm thick). This semi-crystalline polymer was chosen as a coating material because of its chemical stability and resistance to hydrolysis, non-toxicity, high strength and excellent tribological properties, and presently it is one of the most affordable polymers with high biocompatibility (according to the Food and Drug Administration, FDA, agreement) [1,5]. The substrate geometry (wire) was chosen as it is used as guidewires or as a base for medical instruments and implants (i.e. self-expanding stents, filters, baskets, etc.). Previous attempts in coating Nitinol wires with PEEK have been reported [26,28]. In these studies electrophoretic deposition technique was used, but difficulties to achieve a homogeneous coating along the wire with a small surface roughness were encountered; furthermore cracks and ultimately delamination were observed at the high curvature points of the bended wires [26,28].

It is clear that polymer coating on Nitinol can become an interesting direction to explore, only if the biocompatible coated film is stable in physiological fluids and under mechanical constraints. A long-term coating is a necessary requirement of great importance. Here long-term durability is understood twofold. First the substrate/film assembly must be mechanically stable overcoming the often encountered limitation of ultimate film delamination from the substrate immersed in liquids. Secondly, coating integrity must be achieved for biological safety, compatibility, and effectiveness preventing the in-stent restenosis for instance. In our study we show that the coating such as a film is homogeneous, regular in its thickness, adhering perfectly at all high curvature points of the implant architecture (such as encountered in stents, etc.). As a result no delamination, breakdown or fragmentation of coating was observed for PEEK-coated Nitinol wires immersed in liquids for long periods. Moreover the film also keeps the mechanical and shape memory properties of the Nitinol alloy substrates. Our method is based on a systematic optimization of all the parameters governing the successive steps of the alloy surface preparation (cleaning, chemical etching, electropolishing), substrate dipping into a PEEK colloidal solution, and polymer film annealing. In our study we show that the substrate/film assembly quality is mastered by encompassing all the spatial scales from the mesoscopic to the nanometric, both from the chemical and physical points of view. Notably any defects, such as voids, holes, cracks, dewetting areas, permanent sets, formed on the surface of films, in their thickness, or at the substrate/film interface are eliminated. Our method creates excellent film-coated substrate stable in dry, vapor, steam, and physiological liquids, preserving the substrate integrity in an embedded relatively smooth and biocompatible interface.

2. Experimental

2.1. Materials

The investigations were carried out on NiTi alloy intended for implants. Superelastic Nitinol wire alloy "C" of nominal diameter 0.26 mm was purchased from Memry GmbH Nitinol+ (Weil am Rhein, Germany). The wire was purchased straight annealed and the surface was oxidized. Containing nominally a 55.70 wt.% mass fraction of nickel, 44.04 wt.% titanium and about 0.25 wt.% chromium this wire is used for applications where slightly higher stiffness or torqueability is required, such as guidewires and other medical instruments or implants. As the nominal temperature austenite phase graduates from −10 °C to −20 °C, the material was in the high temperature austenitic state at room and higher temperatures. Nitinol wires 3 cm long were used.

Ultra pure water was obtained from a commercial Millipore purification system (MilliQ Gradient system) and used for preparation of the solutions. All acids (HF, HNO_3, $HClO_4$, CH_3COOH) used for pickling and electric polishing procedures were obtained from Sigma Aldrich (Analar grade). The solutions were used as received.

Hanks balanced salt solution was used as a substitute for blood and extracellular body liquids to investigate metal ion release. The Hanks solution (from Sigma Aldrich) had the following composition: $CaCl_2 \times 2H_2O$: 0.185 g/L, $MgSO_4$: 0.09767 g/L, KCl:

0.4 g/L, KH_2PO_4: 0.06 g/L, $NaHCO_3$: 0.35 g/L, NaCl: 8.0 g/L, Na_2HPO_4: 0.04788 g/L, D-Glucose: 1.0 g/L, Phenol red·Na: 0.011 g/L.

Polyether-ether-ketone (PEEK) was purchased from Victrex® Manufacturing Ltd. (South Yorkshire, U.K.) in a water-based dispersion (Vicote® F804; density 1.09 g/cm^3 at 25 °C; pH 6.0). This colloidal dispersion of fine particles (granulometry 10 μm) with a nominal solid value 37.4% has a dynamic viscosity of about 120 mPa s or 110 cSt kinematic viscosity at 25 °C (as calculated from the 20 s elapsed flow-time of the dispersion passing through a 6 mm diameter orifice of a filled flow cup according to the BS EN ISO 2431 standard). It is thermoplastic in nature and exhibits flow above the melt temperature.

2.2. Sample preparation

A homogeneous surface with a reduced roughness was first sought for the Nitinol wires before polymer coating. The procedure removes the initial surface oxide layer formed during the manufacturing process of Nitinol wires, and allows the surface to be polished. This achievement is also necessary to enhance the coating adhesion. The preparation of the substrate surface was obtained in three consecutive steps, all carried out at room temperature (21.0 ± 0.5 °C):

(i) *cleaning* of the surface by immersing the wire in an ultrasonic bath (ELMA FB15050) to get rid of any dirt, organic contaminants and grease. The "sweep" mode was used at a frequency of about 37 kHz during 10 min in acetone and then during 10 min in deionized water. Then the wire was washed in distilled water and dried using filtered compressed air.

(ii) removing impurities from the surface of the metal, inorganic contaminants, rust and oxide layer by *pickling–etching* in strong acid solutions. For this purpose a solution containing hydrofluoric acid HF, nitric acid HNO_3 and water with a 1:4:5 ratio was used. The process of pickling was carried out for each sample separately in a Teflon container. The samples were mounted in a homemade holder and immersed into the solution for different durations (7 min was found to give the best results; see §3-1) at room temperature. During the whole process the solution was stirred with a magnetic stirrer. Then the samples were cleaned in an ultrasonic bath with deionized water for 10 min, and then dried.

(iii) obtaining an oxide layer with a mirror-like finish by *electrochemical polishing*. During this process, the metal from the surface of the immersed sample in electrolyte solution is anodically dissolved by the electric current, which yields to a smooth polished surface. To implement the electrochemical polishing process a homemade cell was built. The wire, which acts as an anode, was positioned vertically in the center of the cylindrical container, made in steel, which acts as a cathode. During electropolishing the sample was gradually rotated around its axis. Electrolyte solution was prepared from 5 mL perchloric acid $HClO_4$ (70%) and 100 mL acetic acid CH_3COOH (65%). Different applied potentials (from 3 to 25 V) and durations (from 3 to 10 min) were examined: the conditions were found optimum when the electropolishing lasted 3 min at 10 V anode potential and 0.3 A/cm^2 current density (see §3-1). After polishing the samples were cleaned in ultrasonic bath with deionized water for 10 min and then dried.

Following our proprietary procedure [35] a regular and controlled roughness at the nanometre scale was then deliberately created on top of the obtained smooth, uniform and homogeneous oxide layer without damaging it. Thus the PEEK film to be subsequently deposited on the wire acquires enhanced adhesive properties. Dip-coating was the final step for PEEK coating the NiTI wires. The wires were immersed into a 37 wt.% colloidal solution of PEEK in water at constant speed, followed by a 2–3 min dwell time in order to leave sufficient interaction time of the substrate with the coating solution for complete wetting. By pulling the wires upward at constant speed to avoid any jitters, a thin layer of precursor solution was entrained, i.e. film deposition. Excess liquid drained from the surface. The wires were left in air for 20 min to allow water to evaporate from the fluid, forming the as-deposited thin film. The immersion and withdrawal processes were conducted in a sealed box at constant temperature 22.0 ± 0.5 °C and relative humidity of 63% in order to avoid any air flow and to prevent premature water evaporation, that would start already during the deposition and drainage steps. The as-deposited thin film was further promoted by heated drying after wire transfer into a preheated oven at 150 °C for 30 min. Subsequently the coating was subjected to further heat treatment: by placing the wires in a preheated oven at 400 °C (just above the PEEK melting temperature) for 10 min the powder polymer particles were sintered, and then by cooling down to room temperature at a −3 °C/min rate, subsequent crystallization was obtained. As a result the coating has a smooth and glossy appearance indicating a uniform, homogeneous, and regular PEEK film in thickness.

2.3. Surface structure characterization

To obtain information on the surface topography and to evaluate surface alterations during each of the procedure steps, Scanning Electron Microscopy (SEM) and Atomic Force Microscopy (AFM) were used. The combination of these two techniques allowed the surface structure of the wires to be viewed at their different preparation stages before coating on all the spatial scales from the mesoscopic to the nanometric. Similarly the quality of the PEEK coating film was controlled at all the spatial scales by tracking eventual voids, holes, cracks, surface inhomogeneities, that would otherwise ultimately lead to delamination of the polymer coating in liquid solutions. SEM observations were performed on wires sticked on glass supports. A conducting 80 nm thick coating gold layer was deposited by sputtering in an argon atmosphere for PEEK-coated wires. The observation of the surface topography was performed on two microscopes operating at voltages ranging from 15 to 25 kV: a Hitachi SU8001 microscope and an environmental microscope Philips XL-30 ESEM equipped with an Everhart-Thornley secondary electron detector. AFM observations were carried out at room temperature in air using a Nanoscope IV instrument (Digital Instruments, Inc., Santa Barbara, CA.). Topographic AFM images were obtained in the contact mode whereas height and phase were obtained by means of tapping mode with microfabricated silicon nitride AFM tips (cantilevers with a spring constant of 42 N/m) and a resonating frequency of about 300 kHz. The scanning rates were varied from 1 to 2 Hz. All SEM and AFM images presented in this work were obtained reproducibly over at least three spots on the sample surfaces around a given position defined by its distance from the wire ends. The wires were scanned along their length to evaluate the variations in homogeneity and uniformity of the surface features. The use of both SEM and AFM allowed the dimensions of the bare and PEEK-coated Nitinol wires to be evaluated at different spots along the wires. Five measuring sites of the wires were arbitrarily chosen to conduct the width measurement, and a mean value was calculated. In addition the estimation of the surface roughness at microscopic scale was determined by imaging different areas of 7 × 7 μm^2 per sample using the root mean square roughness parameter R_a calculated with the AFM software.

2.4. Scratch test

To characterize the surface mechanical properties of the thin PEEK film coating, a Nanoscratch Tester from CSM® Instruments (Anton Paar GmbH) was used. The technique involved generating a controlled scratch (1.2 mm long) with a geometry well-known sharp tip on a selected area parallel to the axis of the wire. Straight PEEK-coated Nitinol wires were attached using Loctite® cyanoacrylate adhesive (Henkel AG, Pratteln, Switzerland) onto glass plates and then fixed in the vice of the instrument sample holder. Their axis was oriented parallel to the displacement direction thanks to a rotary stage at a precision of 1 min of arc, and secured directly underneath the indenter holder in a way to prevent any lateral movement. All scratches were performed by longitudinally moving the wire at constant speed 17 $\mu m\,s^{-1}$. Thanks to the precise alignment every scratch was performed exactly along the summit ridge of the coated wire. Cone-shaped diamond tips (half-apex angle 45°) with a spherical extremity (tip radius R_{tip} = 2 μm with a total roughness R_a less than 10 nm) from CSM® were used. The tip material was drawn across the coated surface under constant or progressive load in the range from 0.1 to 100 mN with an accuracy of 0.03 mN. The apparatus has different attachments: a depth sensing capacitive sensor with an accuracy of 0.01 μm and a friction calibrated table with capacitive sensor (stiffness: 0.64 mN/μm) allowing the tangential force to be also measured simultaneously with an accuracy of 0.06 mN. During the scratch test, the displacement of the wire as well as the applied normal force (F_n) are controlled. The tangential force (F_t) and penetration depth were continuously recorded using a data acquisition system every 20 ms (50 Hz).

All measurements were conducted at ambient temperature in an air-controlled laboratory with a temperature variation stable at 0.5 °C/h. As an entire scratch process lasted less than a few minutes thermal drift was negligible. Each scratch test was performed twice to insure repeatability of results and the overall variation was found to be less the 10%.

2.5. Biocompatibility

2.5.1. Ion release

PEEK-coated NiTi wires were immersed in Hanks solutions for different periods ranging from several days to one month. Each wire was placed in a separate carefully sealed polypropylene cuvette at 37.0 ± 0.5 °C. The specimen surface area immersed in the 1.3 mL Hanks solution was about 14 mm^2. After an incubation of 12, 18, 24, and 31 days, the wires were removed and the contents in nickel of the solutions were analyzed by Inductively Coupled Plasma Mass Spectrometry using an Agilent 7500 ICP-MS® with a relative experimental error not exceeding 2–3%.

2.5.2. Cell cultures and analyses

Prior to any biological use, each wire (PEEK-coated and bare treated but not coated Nitinol control wire) was fixed to a 16 × 16 mm glass cover slide with a drop of paraffin; they were submitted to UV sterilizing treatment in dry 6 well plaques under laminar flow cell culture hood, then washed in sterile phosphate buffered saline (PBS) before preincubation in standard cell culture media for 2 to 4 h at 37 °C, ending by a second UV sterilization cycle. After media changes, cells were seeded at desired concentration within test and control wells respectively.

2.5.2.1. Cell growth. PEEK-coated samples and Nitinol-controls were tested in duplicate (or more). Murine fibroblast NIH/3T3 (ATCC® CRL-1658™) isolated from Swiss strain embryos, were cultured for tests of cell viability, adherence and standard growth, in Dulbecco's modified Eagle medium (DMEM) high glucose growth media, with 10% heat inactivated fetal calf serum (FCS), and 1% Penicillin-Streptomycin. Cells were seeded at 5×10^4 cell/mL (for 24 h growth), or at 5×10^3 cell/mL (for 48 h and 9 day cultures), and they were grown at 37 °C in 5% CO_2 humidified atmosphere, with medium changes performed every 2 days.

2.5.2.2. Cell imaging. Cells were fixed with 3.7% paraformaldehyde and permeabilized with 0.1% Triton X-100. Rhodamin-labeled phalloïdin (#77418-1EA, Sigma-Aldrich) at 0.005 mg/mL final concentration was used for cytoskeletal F-actin visualization, and samples were mounted on glass slides using Vecta-shield DAPI (4′,6′-diamidino-2-phenylindole) containing mounting medium (#H-1200, Clinisciences) to allow nuclear DNA labeling. A Confocal Zeiss LSM 710 was used for image documentation.

3. Results and analysis

3.1. Optimization of the parameters of the procedure steps

In this study the core experimental problem has been to promote adequate macroscopic NiTi surfaces to be used for coating a thin PEEK film with a uniform thickness and a homogeneous microstructure along the wire length that is stable in biological environment. Our previous works on similar substrates have shown that the best adherence is obtained when the substrate is prepared with the most homogeneous surface microstructure over macroscopic areas together with a reduced and controlled roughness [35]. To accompany us along this route we used the combination of SEM and AFM techniques to monitor the surface topography at every step of the process upon preparation of the substrate. In particular we sought the elimination of all unnecessary relief and surface physical defects such as indentions, grooves, peaks, ridges and asperities, foreign particles, to increase the wettability of the PEEK colloidal suspension that will be deposited ultimately. To achieve this goal we systematically optimized all the parameters governing the aforementioned three successive steps in substrate preparation.

Surface of as-received Nitinol wire has a dark color due to the thick oxide layer formed during its manufacture upon repeated drawing through dyes of various sizes. This raw surface is rough, inhomogeneous and has many defects as evidenced by SEM (Fig. 1). A structure aligned in the direction of deformation can be noticed. Surface physical defects like indentions, grooves from drawing, scale, as well as foreign particles can be seen. Usually the black oxide is removed by sandblasting. We preferred not using the sandblasting procedure as it leads to a nonhomogeneous surface with unorganized texture. Rather we followed the simplest procedure developed in earlier X-ray photoelectron studies of as-cast Nitinol alloys [36] and wires [18,37] where it was shown that surface quality could be tremendously improved. Cleaning with acetone and deionized water is important for the preparation of samples for further processing: greasy films and various contaminants are removed from the surface providing a contact with acid solutions more uniform upon subsequent chemical etching. Thus, the first step consisted in cleaning each wire ultrasonically in successive baths of acetone and deionized water for 10 min for each procedure, followed by drying using filtered compressed air.

Chemical etching in a HF/HNO_3 solution was used to clean the surface physically, to eliminate surface scratches, to remove highly deformed defect material, to oxidize the surface, and to leach the nickel [18,36–38]. The latter is revealed by the observed green color of the etching solution indicating the presence of Ni^{2+} ions. Fig. 2 shows the SEM images of a Nitinol wire surface after pickling in a $1HF + 4HNO_3 + 5H_2O$ solution for different durations of the process. A crater-like morphology with crater diameters in the range of 1–5 μm and about half a micrometer in depth is a typical surface

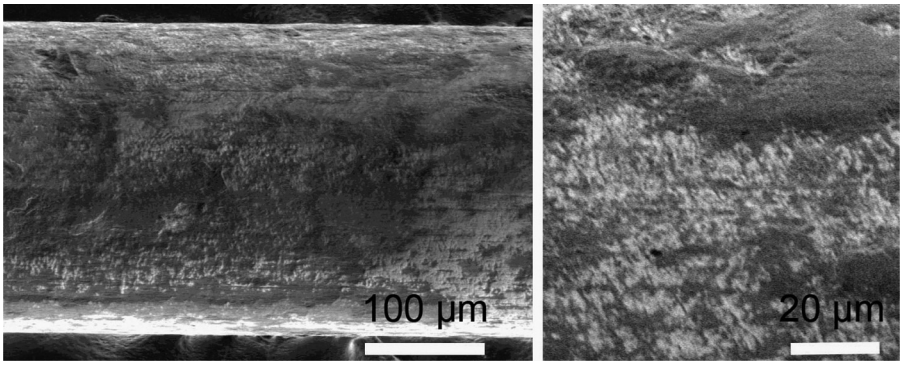

Fig. 1. SEM images of a Nitinol wire in the as-received state revealing a very irregular and porous surface topography.

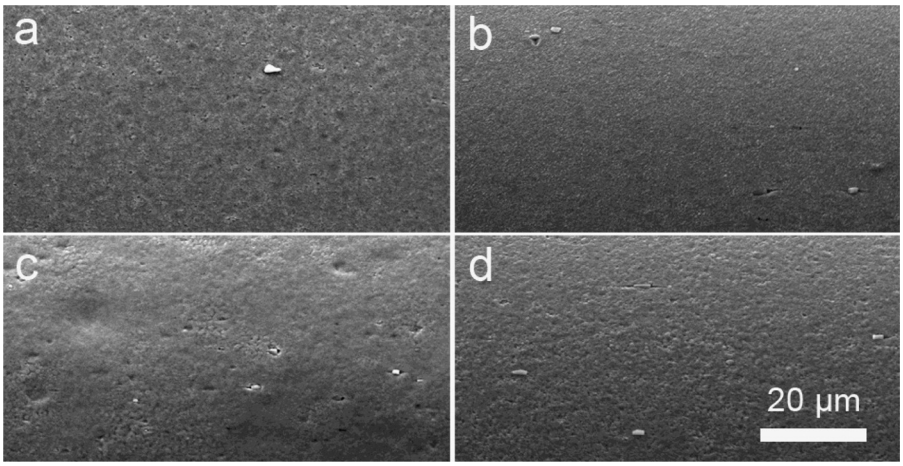

Fig. 2. SEM images of a Nitinol wire surface after the acid pickling process that lasted for 6 min (a), 7 min (b), 10 min (c), and 15 min (d). The major features of the surface topography on a micron scale are crater-like indentions. Note the white spots of 2–6 μm size (see text).

appearance after chemical etching [18]. These crater-like pores or indentions can be either single or in clusters. They have smooth walls in contrast to the deep and sharp grooves and cracks observed on the wires in the as-received state (compare with Fig. 1). White particles of 2–6 μm size could also be observed on the surface after chemical etching. They were either embedded into the surface or spread on the surface. These were also reported in previous studies [18], and interpreted as lenticular precipitates of second phase due to cold work and multiple annealing formed during the processing of wire [39].

To find the optimal conditions we varied the duration of the process in the range from a few minutes up to 15 min. It appears that 7 min is an optimum duration for the process as it allows sufficient time for the oxide layer dissolution. Moreover the surface is the most homogeneous and the smoothest. Indeed, if the samples are kept in acid solution for a shorter period of time, the entire oxide layer is not fully removed as it can be noticed when imaging the surface (Fig. 2a). Conversely with an increasing pickling duration in the range 10–15 min the acid begins to attack the alloy underneath as it can be inferred from the decrease of the wire diameter (Figs. 2c,d). The images reveal also deep pits, surface cracks and surface fragments: in short the substrate surface gets less uniform and acquires an increased roughness.

The next step for surface preparation is electropolishing. During the procedure of electrolytic polishing a balance is achieved between the formation of a passive layer and the dissolving of the surface region into the electrolyte. This leads to a favored removal of roughness tips. Thus by means of electrolytic polishing, smooth surfaces can be prepared: this is of great interest for the preparation of a substrate surface with a very fine structure for subsequent coating. Numerous electrolytes have proved satisfactory in metallography and electropolishing; among them we chose the electrolyte made of perchloric acid mixed with acetic acid as it was previously used for electropolishing Nitinol [38,40,41] and reported to give the best results for processing NiTi in the austenitic structure state at room temperature [40].

Note that if the etching step is skipped and electropolishing step is only proceeded, the homogeneity of the surface may be even lower than it was from the start, where rough oxide layers may still adhere to the substrate surface; this observation is in agreement with previous reports [38]. This means that the natural oxides cannot be removed only by electrochemical polishing without using etching pretreatment by acid. To find the best optimal polishing conditions the influence of several parameters was evaluated: applied voltage (and therefore current density), duration, the use or the non use of a magnetic stirrer during the process, which provides additional electrolyte flow in the system and consequently may cause a decrease in the concentration of metal ions in the vicinity of the wire surface. Initially, several values of applied voltage 3, 5, 10, 15 and 25 V were tested with a fixed duration of 3 min and the surface morphology after the procedure was investigated by SEM (Fig. 3). Then, with the same anode potential values electric polishing was conducted at longer durations of 5 and 10 min.

A characteristic feature of electrochemical polishing is smoothing the metal surface by intense dissolution of the small protuberances. As revealed by SEM (Fig. 3) and AFM (Fig. 4), the quality and outcome of electropolishing strongly depend on the parameters under which the process was held. Actually, polishing

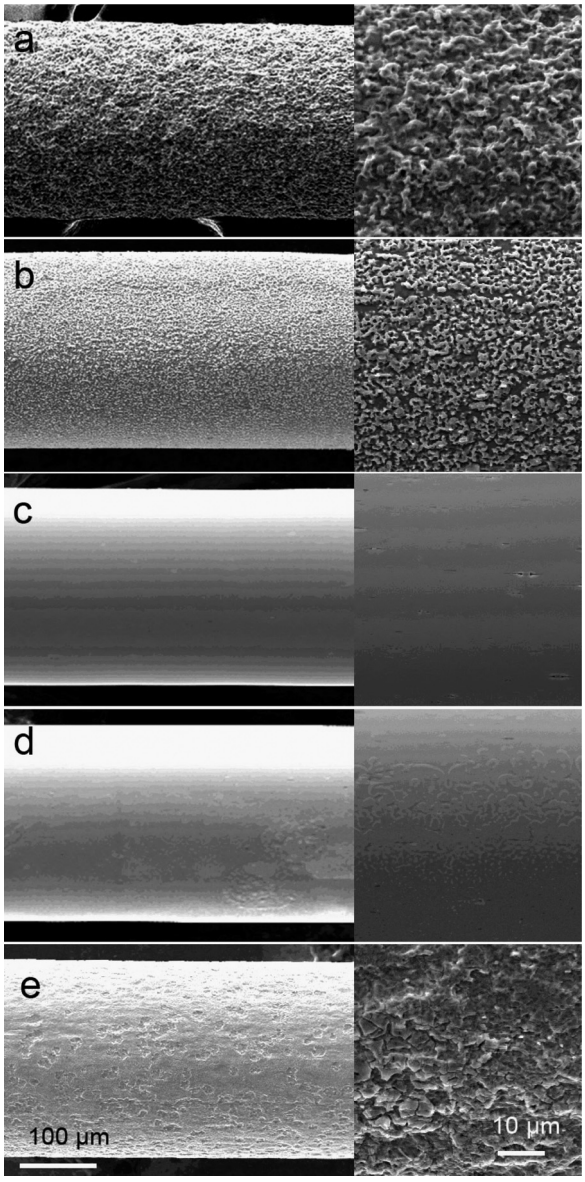

Fig. 3. SEM images of a Nitinol wire surface after electrochemical polishing for 3 min using a voltage of 3 V (a), 5 V (b), 10 V (c), 15 V (d), and 25 V (e). The best leveling of the surface topography is obtained in the plateau region at 10 V and 0.3 A/cm^2 (c): bright, microscopically smooth and flat surfaces of the "mirror" glance are obtained free of stress, scratches and occlusions, even if occasional pits of small size and inclusions and voids around the inclusions may remain (c right; enlargement).

took place in a narrow range of applied voltage (around 10 V) and hence of current intensity. The current density vs. voltage curve shows a polishing plateau (around 0.3 A/cm^2; a value in agreement with ref. [40]) at room temperature for this electrolyte, and indeed the best results according to SEM were achieved in the middle range of this plateau (Fig. 3c). Operating at this plateau the leveling of the surface topography converges to a stationary smooth condition. The surface is the most flat, smooth and uniform (Fig. 3c). Increasing the voltage (and hence the current density) beyond the plateau (>12 V) is not of any help and regrettably would have the opposite effect to what is intended: not only the substrate is thinned but at the same time the surface topography is effected as the roughness is steadily increased. At the plateau level the linear solution rate of about 3–4 μm/min enables the setting of the requested removal of surface material. We set the process duration at about 3 min. Increasing polishing times is unnecessary and may induce the formation of waves at the surface which are due to the different solution behavior within the material zones stretched in the shape of bands as a result of deformation [40]. Although some authors note that stirring the electrolyte has a negative outcome [38], in our experiments we observed the converse: the electrolyte solution gently mixed with a magnetic stirrer during the electropolishing process yields to a surface polished more evenly. The vortex speed could indeed induce complex effects. Electropolishing resulted in microscopically smooth surfaces, free of stress and occlusions, most often of the "mirror" glance.

The morphology of the sample surfaces as studied using the high resolution SEM can also be investigated at a microscopic scale by AFM. In particular, the "mirror" glance of the Nitinol wires after treatment is confirmed quantitatively by measuring the mean roughness factor R_a of the surface. Fig. 4 compares the topographic images obtained by AFM in contact mode for the same Nitinol wire before and after treatment using the best optimum conditions of the three consecutive steps as described above. These images were found to be representative at microscopic scale along a given wire and when repeating the measurements on different wires. The root-mean-square height deviation calculated for scan areas of 7×7 μm, decreases by a factor 5: it is 21 nm for the as-received NiTi wire and only 4 nm for the almost flattened surface after electropolishing in the plateau region (see Fig. 3c). Thus the obtained surfaces after treatment appear highly smooth, very uniform, and lustrous practically everywhere, with a difference between the real and geometric surface area not exceeding a couple of percents. This confirms high quality of the electrochemically polished surface of the Nitinol alloy.

Taking advantage of the high quality of the electrochemically polished surface of the Nitinol alloy, in terms of smoothness and uniformity, deposition of a thin PEEK film can now be carried out. We followed our well established procedure in different systems for obtaining a high quality polymeric coating on the substrate [35]. First a regular and controlled roughness at the nanometre scale was added on top of the electropolished surface of the wire without affecting its oxide layer [35]. This allows the PEEK chains to get attached efficiently to the substrate as entanglements are favored. As a result a strong adhesive coating film will be obtained (see §3-2). The dip-coating procedure was chosen since flame-spray and electrodeposition techniques showed drawbacks for PEEK deposition on wires [26,28]. The withdrawal speed of the wire from the 37 wt.% colloidal solution of PEEK in water is the governing parameter for the ultimate thickness of the coated film. Film thickness is determined by the competition between surface tension (capillary force), gravity and viscosity. As a rule of thumb the slower the substrate is withdrawn, the thinner the film deposited. Thus according to the Landau-Levich-Derjaguin theory, for a plate substrate withdrawn from the bath of coating at constant speed V, the layer thickness h, which remains on the surface, follows a power-law $h \sim \left(\frac{\eta V}{\gamma}\right)^{2/3}$ where η is the liquid viscosity and γ the surface tension [42,43]. On the other hand, thicker films may also be obtained if the capillarity regime is applied, where very low withdrawals speeds are used. Here solvent evaporation becomes faster than the movement of the drying line leading to a continuous feeding of the upper part of the dynamic meniscus and finally also to thicker films.

For a substrate with a cylindrical geometry such as a fiber or a wire (radius r), the coating thickness is given by [44]:

$$h = \frac{1.34 r \mathrm{Ca}^{2/3}}{1 - 1.34 \mathrm{Ca}^{2/3}} \quad (1)$$

where $\mathrm{Ca} = \eta V/\gamma$ is the so-called capillary-number. Here, gravity is neglected since the Laplace pressure is much larger than the hydrostatic one. Indeed, for a Nitinol wire of radius $r = 0.13$ mm the Bond number, which compares gravity and capillary forces, is

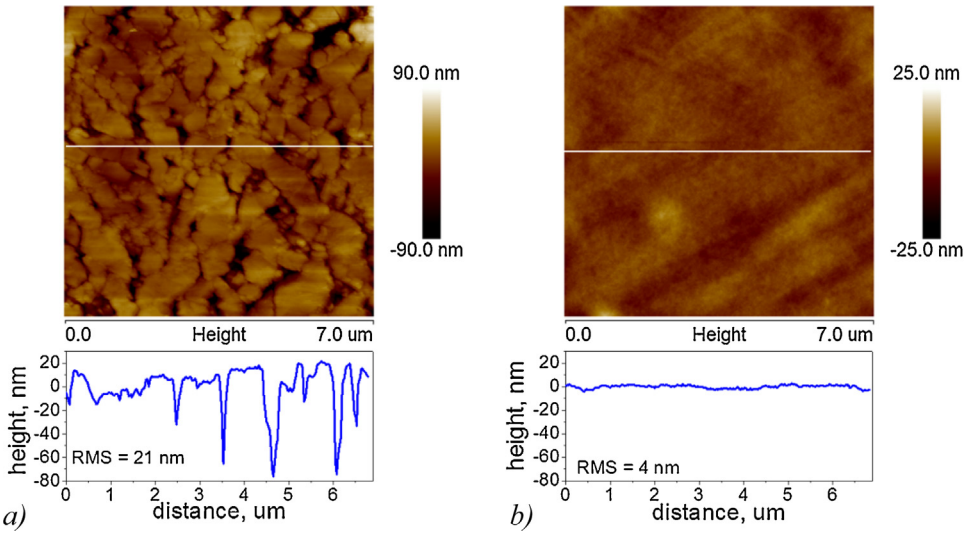

Fig. 4. Contact mode AFM topographic images of a Nitinol wire (a) as-received and (b) after electrochemical polishing in the plateau region (see Fig. 3c). The bottom plots show the profile roughness drawn along the horizontal white line outlined in the center of the AFM images. The root-mean-square height deviation calculated for the 7×7 μm area is 21 nm (a) and 4 nm (b).

$Bo = \rho g r^2/\gamma = r^2\kappa^2$ (with ρ the liquid density, g the gravity acceleration, and κ^{-1} the capillary length) of the order of 7×10^{-3} much smaller than 1. In this work we sought to get PEEK coating films not thicker than 15 μm, to retain the superelasticity property of the Nitinol wire. Having $h/r \leq 0.1$ implies that Ca is not larger than 0.02 and hence the coating velocity must be around a few mm/min. In this regime one note that two effects can be neglected. On one hand the coating velocity is slow enough to avoid inertial effects: the Weber number $We = \rho V^2 r/\gamma$, which compares inertia to capillary force, is negligible (of the order of 10^{-8} to 10^{-7}). On the other hand the coating velocity is not extremely slow and the role of intermolecular forces, such as the long-range van der Waals interactions (about 100 nm range), can also be ignored [45]. As a consequence equation (1) is valid and $h \approx 1.34 r Ca^{2/3}$ showing that the film thickness results from a balance between capillarity and viscosity.

In this visco-capillary regime, low velocities correspond to thin films, and it is logical that the interfaces play a key role. The solid-liquid interface entrains matter because of the liquid viscosity, but the liquid-air interface can also do this as surfactants are present in the PEEK solution for stabilizing the colloidal suspension. It is known that the latter (even in small proportions) may provoke a thickening of the entrained film, if compared with coating from a pure liquid of the same viscosity and surface tension [45]. The simplest analysis of this thickening effect consists in supposing that the free interface moves at the same velocity as the substrate, leading to $h = 1.88\,\kappa^{-1} Ca^{2/3}$ (Frankel's law) [45]. The effect is caused by the Marangoni flow that takes place when drawing the solid substrate out of the solution, and its magnitude results from a balance between convection (which causes the thickening) and adsorption from the volume (which may erase the surface gradient). All these effects as well as the non-Newtonian effects of the colloidal solution complicates the predicted coating thickness at a given velocity. Nevertheless, we have used the above equation (1) as a guide for optimizing the desired coating thickness on the Nitinol wires.

After the substrate withdrawal from the bath of coating the fluid film on the wire may become unstable. This is due to the liquid surface tension that spontaneously undulates and finally may break into a (periodic) array of droplets. These Plateau-Rayleigh instabilities are emphasized for the wavelengths larger than the circumference $2\pi(r+h)$ of the fluid cylinder. Typically the characteristic time scale of the instability scales as $\eta r^4/\gamma h^3$ [45] which is 10^4 times longer than the formation time of the film ($\sim \eta r/\gamma Ca^{2/3}$).

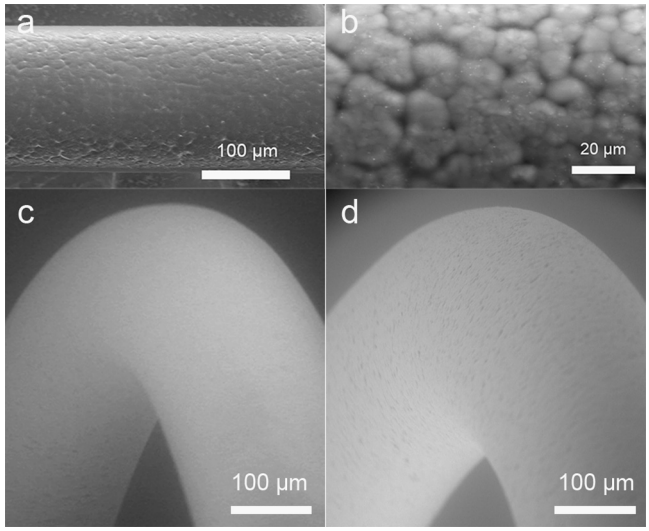

Fig. 5. Scanning electron microscopy images of sintered PEEK-coated NiTi wires at different magnifications. The coating film is continuous and homogeneous along both the straight (a) and bent parts (c,d) of the wire. The high magnification reveals spherulites as expected for the semi-crystalline PEEK (b). Note its thickness uniformity even around the high curvature points of the U-shape part of the wire that was curved into a spring prior to coating. No difference was noted before (c) and after (d) immersion in Hanks solution and for 83 days where the wire was repeated periodic compressing and stretching cycles.

The dynamics of the instability is completely decoupled with the film formation, especially as the deposited film was annealed just after coating. Thus a slow evaporation of water from the fluid was allowed when in the same controlled humidity enclosure the wire was held in air at RH 63% for 20 min just after its withdrawal from the bath of coating. Then the wire was transferred to a preheated oven at 150 °C and further heated drying was carried out during 30 min. Since the as deposited PEEK coatings were fragile and easily flaked off the substrates, a sintering step was needed to increase the adherence to the substrate and to enhance the deposit mechanical properties. Thus the wires were carefully transferred to another preheated oven at 400 °C (above the PEEK melting temperature). An holding time of 10 min allowed the polymer particles to be sintered and a uniform film covering the whole surface to be obtained.

Note that these successive steps for annealing the dip-coated PEEK film had been optimized in other works [35]. Thus, the parameters used for the slow evaporation of water from the fluid, the heated drying, the sintering and the ultimate crystallization by slow cooling down to room temperature (cooling rate: −3 °C/min) were all kept constant, leaving the coating velocity as the main remaining parameter to be optimized.

Thus our task was to obtain a uniform complete coverage of the wire at any spatial scales (from micrometric to nanometric scales) without any defects, cracks or holes, and with a sufficiently thin layer that could allow the superelasticity of the Nitinol wire to be retained. SEM images of PEEK-coated NiTi wires are presented in Fig. 5. With the conditions aforementioned for drying and subsequent thermal sequences the best quality in terms of homogeneity and uniformity for the coating film was obtained with a withdrawal speed around 63 μm/s (Fig. 5a). Note that the velocity value for immersing the wire in the PEEK colloidal solution is not an important parameter: the immersion speed can be varied over a large range without affecting the quality of the ultimate coating (we used a speed around 150 μm/s). The coated PEEK film is regular in its thickness (12.0 ± 0.2 μm) all along the straight wire length (3 cm long), with a substrate being completely covered without any cracks, defects and holes. A large magnification reveals the characteristic spherulitic microstructure of the semi-crystalline PEEK [46], which indicates that the polymer melting and subsequent crystallization process have been actually successful (Fig. 5b). The fine grained mosaic structure has a size and density of spherulites, that depend on the processing conditions from the melt [47]; here the lamellae of the PEEK crystals are organized in spherulites of about 10–20 μm in diameter.

One important advantage of using dip-coating is that the topography of the resulting film surface is continuous and homogeneous, even in curved geometries that are more complex than straight wires. Thus our procedure was applied for bare helicoidal springs built by twisting Nitinol straight wires prior to dip-coating. The open coiled helical springs were 30 mm long (17 coils) and had a 4 mm mean diameter, a value close to diameters used in coronary stents. For this geometry (and topologies even more complex, such as saddle shapes, that we have already started to process) the predetermined aforementioned parameters for the dipping procedure set in the case of straight wires are not always fully adequate. Indeed, we have encountered difficulties during the coating process as the high viscosity and density of the colloidal PEEK solution induce some undesired accumulation of material in the zones of high curvature. To overcome these drawbacks we used a large number of combinations including simple variations of the solution concentration, the withdrawal speed and the angle of inclination of the specimen to be withdrawn from the precursor solution. A full report of this method for coating wires in more complex geometries and topologies will be detailed in a forthcoming article. The coated film on coiled helical springs reported here appeared continuous, uniform, homogeneous, with a regular thickness all along its length even along the U-shape parts encountered (Fig. 5c), although we noted a slightly larger variation in thickness (12.0 ± 0.5 μm) compared to straight wires (12.0 ± 0.2 μm). The quality and uniformity of the material preserved the thermo-mechanical properties of the Nitinol wire, including stress and fatigue behavior.

These claims are supported by several investigations of the mechanical response of the coated substrates via a homebuilt device for making uniformly stretched (radially compressed) the helical springs. Stretching one spring in the axial direction was obtained by attaching the two ends of the wire to end plates with clamps. The drive train accommodates the end plates (protected with Teflon to avoid contamination) and the electronic control system imposes a predetermined velocity on one or both of the end plates. The sealed chamber of the apparatus allows the helical springs to be immersed in fluids for considerable periods of time without any evaporation or contamination. The geometric dimensions and motor capacity of the motion-control system determine the range of experimental parameters accessible in a given wire-stretching experiment (total travel available to the motor plates, maximum velocity and time-dependence of the oscillatory movement the motor can sustain; note also that the operating space accessible with a given fluid can also be further constrained by instabilities associated with capillarity and gravitational sagging). Full details will be given in a forthcoming article. Using this home-built device we first compared the load-displacement curves in loading and unloading for both bare and coated NiTi wires. No differences were noted suggesting that neither the presence of a coating of around 12 μm in thickness nor the eventual effect of heat treatment (400 °C for 10 min) effect the superelastic behavior of the nitinol wires (see also the discussion in § 4-2). In other experiments the coiled helical coated substrates immersed in a physiological medium (Hanks solutions) at 37 °C were subjected to a mechanical stress in continuous cycles of axial compression/stretching at 20% strain for 7 million cycles (equivalent to a heart rate of 60 beats per minute). Neither the film appearance, its structure, nor its adhesion were altered after more than two months: no cracks were visible and no delamination occurred (Fig. 5d).

3.2. Adherence of the PEEK coating film

The nanoscratch scratch test is a useful technique to investigate the surface mechanical resistance of thin coatings and their adherence to a substrate [48,49]. For PEEK-coated NiTi wires, the great advantage of nanoscratches is the small size of the indenter (tip radius R_{tip} = 2 μm) smaller than the PEEK film thickness (12 μm). The entire scratch process was divided into three main phases: (i) acquisition of initial topography (pre-scratch phase); (ii) the scratch cycle itself (i.e., controlled loading and unloading) to be detailed below; and (iii) acquisition of the residual groove topography (post-scratch phase). The contact point where the tip touches the sample surface is chosen by optical microscopy and then used to calculate the depth of contact. From this contact point, the scratch cycle itself was initiated. These three consecutive phases, all carried out at the same steady scratch speed of 17 μm s^{-1} are now described more in details:

(i) *pre-scratch phase:* during this phase the tip was loaded to the nominal load F_n = 0.1 mN. A displacement of the tip was imposed to access to the initial topography of the sample. The length of the scanned zone along the summit ridge of the wire axis was 1200 μm (100 μm before and 100 μm after the 1000 μm region long where the scratch test will be done). At the travelling end the tip was moved laterally, then the sliding movement was reversed, and after 1200 μm, the tip was moved back laterally to return to its initial starting point. The sequence carried out during this pre-scratch phase allowed height difference of up to 40 μm over 1200 μm (3.3% tilt) to be detected and instrument reference to be adjusted.

(ii) *scratch phase:* an initial displacement of 100 μm of the tip onto the surface was proceeded at the nominal constant force F_n = 0.1 mN. Then, over the next 1000 μm the normal load was linearly increased from 0.1 mN up to 100 mN. At the end the last 100 μm were again traveled at the nominal value of 0.1 mN. The return to the starting point was proceeded as in the pre-scratch phase.

(iii) *post-scratch phase:* the topography of the same overall zone was measured as in the pre-scratch phase (F_n = 0.1 mN). This sequence allowed the mechanical recovery of the sample surface and the residual scratch groove to be investigated.

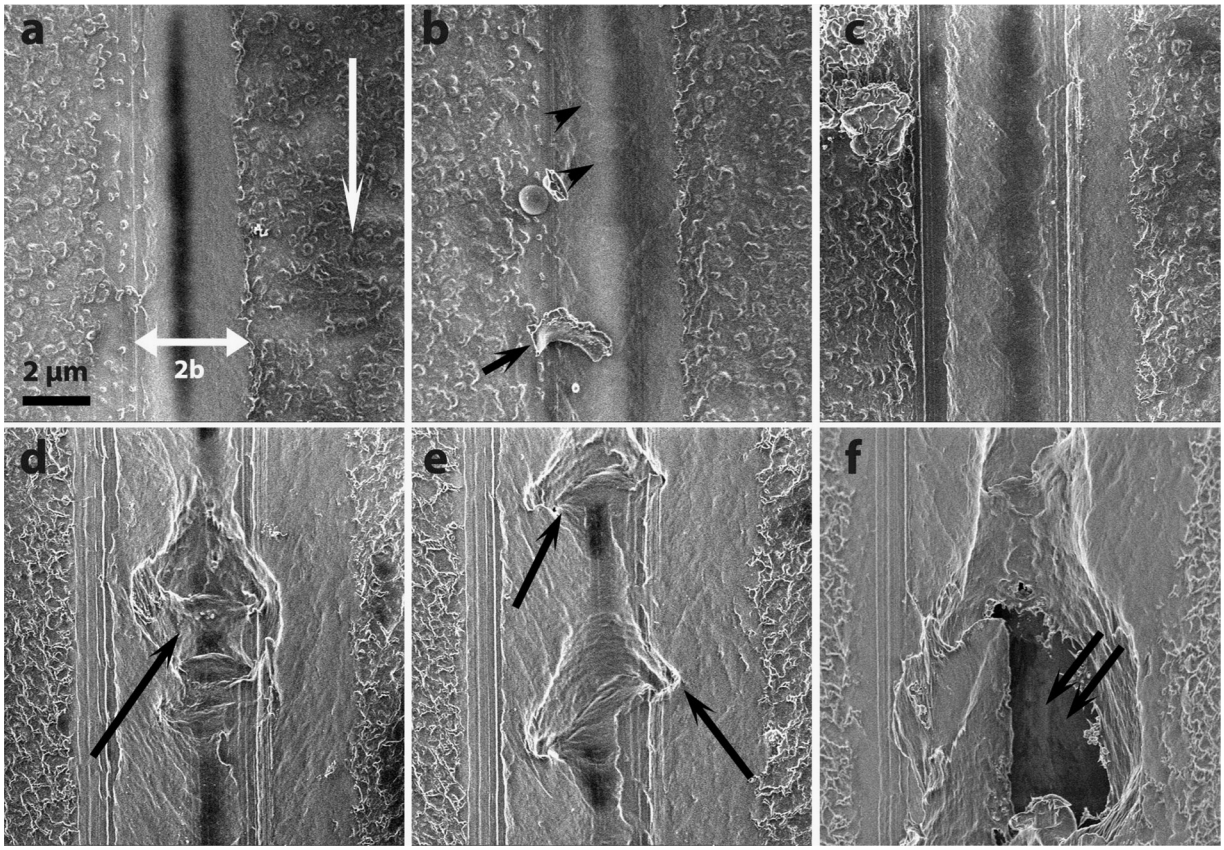

Fig. 6. SEM observations of the scratch groove formed on a PEEK-coated Nitinol wire. The micrographs (a) to (f) are taken at the same magnification at different locations along the track and correspond to increasing applied loads, F_n. For each micrograph the sliding direction goes from the top to the bottom as indicated by the white arrow in (a) and the groove has a continuous varying width, 2b, due to the conical shape of the indenter penetrating deeper into the film as the applied load linearly increases with the sliding. (a) $F_n \approx 30$ mN: the deformation is plastic. The black stripe is due to charge effects; (b) $F_n \approx 34$ mN: as the applied load increases concave superficial cracks are created in front of the tip contact (black head arrows) and some film fragments may be torn away (black arrow); (c) $F_n \approx 48$ mN: with a larger normal force the arcs become more pronounced reversing their shape to convex or presenting a zig-zag pattern and the detached debris contribute to a three-body abrasion and induce worn traces as the indenter tip further progresses; (d) $F_n \approx 74$ mN: cohesive defects (black arrow) of the PEEK film appear above a critical mean pressure applied onto the film; (e) $F_n \approx 79$ mN: consecutive cohesive defects (black arrows) correspond to a periodic initiation/propagation of cracks during the fracturing process (see the peaks in the F_t vs F_n curve in Fig. 7); (f) $F_n \approx 97$ mN: the cohesive defects of the PEEK coating film have reached the interface between the NiTi substrate and the layer (double black arrow) without delamination.

The surface features and residual grooves created by scratch tests on the coated surface were observed and measured by SEM after the scratch cycle was performed (Fig. 6). At the beginning of the scratch an elastic behavior characterized by the absence of scratch tracks is observed. Thus no additional features distinguishable of the general texture of the film is noted: only the characteristic texture of the PEEK film comprised of spherulites can be seen by SEM. This high recoverable elastic deformation continues for long as the increasing applied force is low enough. However, as soon as F_n becomes larger than about 25 mN (i.e. ≈250 µm from the scratch beginning) a groove trace becomes visible. It is revealed with ridges oriented along the sliding direction, i.e. the wire axis (Fig. 6a). This indicates that the deformation has become irreversible due to a plastic flow of material in the sliding direction. From this point the groove deepens with a continuous varying depth due to the linearly increased applied load, F_n (Fig. 7). As a consequence of the indenter spherico-conical shape, the groove width, *2b* (as measured from the SEM micrographs, Fig. 6) also widens continuously. In front of the indenter tip microcracks develop due to friction between the indenter and the tested surface, and extend perpendicular to the sliding direction (Figs. 6b and 6c). These microcracks are a superficial event and have no interaction with the substrate interface. The applied load being sufficiently large may also tear away some fragments from the film. The produced debris may further slide together with the indenter and create additional grooves along the ridges of the main groove in the following sliding process (Figs. 6b–f). All these additional scratches and grooves are a result of ploughing action by the counter-face and/or loose wear debris as third body abrasion. The ridges that form around the grooves subsequently deform and fracture to generate new wear debris. It is found that these series of parallel grooves are more prominent at high normal load (compare Fig. 6b with Fig. 6d–f). At some point, peeling or chipping of the coating film can be observed. This corresponds to a threshold in the applied normal load, $F_c \approx 40$ mN, beyond which the effect is exacerbated. Thus SEM examination of the second part of the track subjected to loads larger than F_c reveals evidence of cohesive defects of the PEEK coating film. Above this critical load, F_c, the coating film starts to fail due to the pure plastic behavior of the film under large applied loads. Here collated with SEM observations, this critical load can also be confirmed with the measurement of the tangential force, which becomes to fluctuate widely (Fig. 7). Consecutive cohesive defects, as observed in Fig. 6e, correspond to a periodic absorption/release of energy during the fracturing between two consecutive secondary maxima in the F_t vs. F_n force curve (Fig. 7). Deformations lag behind the load as the indenter continues penetrating into the film. The larger the normal load the higher density of cohesive defects in the scratched PEEK film. Ultimately the cohesive defects reach the interface between the coating film and the NiTi substrate and support exposed portions are revealed (Fig. 6f). Note that the baring

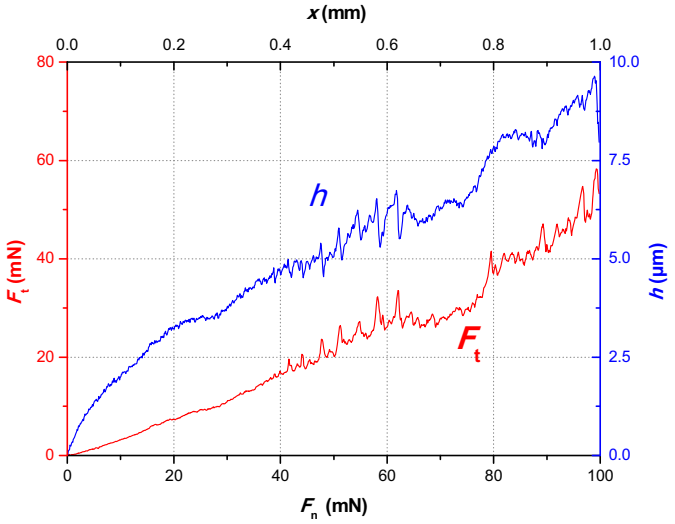

Fig. 7. Profiles of the penetration depth (h) and of the tangential force (F_t) monitored as the scratch processes along PEEK-coated wires. The normal applied load F_n increases linearly from 0.1 to 100 mN along the 1000 μm scratch (spatial coordinate x). Three regimes can be distinguished. At low normal loads the scratch trace is invisible (x < 250 μm) and the behavior is purely elastic. A transition to an elasto-plastic behavior occurs at $F_n \approx 25$ mN and a groove is irreversibly formed (see Fig. 6). Above a critical load threshold around 40 mN the behavior becomes plastic with formation of cohesive defects occurring periodically with an initiation/propagation of cracks during the fracturing process.

of the Nitinol surface does not result from the delamination of the PEEK coating film, but from the collapse of its cohesion only. Indeed, delamination usually occurs due to heavy plastic deformation of the surface layers, nucleation of subsurface cracks, where shear stress is maximum, and propagation of these cracks parallel to the surface and as a result, sheet-like wear particles are generated [48,49]. None of these features were observed.

As a conclusion the thin coating film appears to adhere extremely strongly to the NiTi substrate, since a normal load larger than 100 mN, which corresponds to a mean pressure of about 2.2 GPa (see § 4–2 Discussion), was not able to peel it off. Remarkably this adherence is not weakened after long-term immersion of PEEK-coated NiTi wires in Hanks solution for which the same sequence of surface features was observed upon nanoscratch test. These results indicate that our process of coating Nitinol wires with a thin PEEK film has been very successful.

3.3. Biocompatibility

3.3.1. Ion release analysis

One of the informative methods to determine the stability of metal corrosion is to estimate the number of ions that leach out into the surrounding biological environment. Speed of release of metal ions and their activity determines the potential toxicity of implantable medical devices [50]. The corrosion performance of biomedical materials is more commonly evaluated using simulated physiological solutions rather than actual physiological liquids. In general, the simulated solutions are based primarily on the salt content of the actual physiological solution. Among the different solutions that are commonly used to simulate blood and other physiological liquids in corrosion tests, we chose Hanks solutions for the investigation. The PEEK-coated NiTi wires left at 37.0 ± 0.5 °C for different incubation periods (12, 18, 24, and 31 days) released negligible metal ions as measured by Inductively Coupled Plasma Mass Spectrometry (ICP-MS). From the cumulative and differential Ni concentrations a mean value of the Ni release rate can be estimated. Averaged over the first 12 days, the Ni release rate was less than 1.4 ng/cm^2/day that is a mean rate 10–100 times smaller than the ones reported for passivated [16] or chemically etched Nitinol [51]. After longer immersion periods the mean release rate was even slower. It was divided by a factor 4 after a period that was doubled: this low level rate appears to be of the same order of magnitude with what was observed with electropolished stents (0.4 ng/cm^2/day after 17 days in Hanks solution as reported in [17]). After one month the Ni content maximum concentration was still below the level (<3 ng/mL) considered to be normal: for comparison the nickel content in drinking water is about 20 ng/mL and the average nickel intake by non-occupationally exposed adults varies from 0.1 to 0.9 mg per day where the main exposures results from food (100–250 μg per day), drinking water (up to 20 μg per day) and cigarettes (4–8 μg per 20 cigarettes) as summarized in a recent European Risk Assessment Report [52]. Note that the decrease in nickel release rate cannot be due to saturation effects of Hanks solution as similar values were obtained when the solutions were refreshed. The Hanks solution in which the mechanical cycling test was performed during 83 days was also analyzed after completion: the Ni content had similar low values. All these results show the efficiency of the surface oxide and the PEEK film as a protective coating.

3.3.2. Fibroblast cytotoxicity and cytocompatibility

Cells were followed and observed at 24-, 48-h, 3, 7 and 9 days of culture; there was no difference in appearance between those which were in the presence of PEEK-coated Nitinol wires and those of the control cultures with bare Nitinol wires. At confluence, both the 9 day assay and control cultures contained a homogenous cell monolayer covering the surface of the culture wells and in contact with the wires, plus round unattached cells floating in the culture medium, showing that the cultures had matured without any cytotoxicity. A few sparse fibroblasts were attached lying on the PEEK-coated and bare Nitinol wires.

Fig. 8 shows confocal fluorescent microscopy images of fibroblast cells after 24 h culture in presence of a PEEK-coated NiTi wire, with a top view of the field at left, and a 3D reconstruction at right of the figure. The experiments show that the PEEK film support the growth of fibroblasts with no zone of inhibition of cell growth around the coated wire. The attached cells have an elongated shape but do not have any preferential orientation. The statistical distributions of attached cells on PEEK-coated NiTi wires were similar to those calculated on bare control nitinol wires, once they are normalized by the initial cell density. Note that analysis of the protein and cell adhesion on PEEK surfaces are only possible to a restricted degree since PEEK has a significant inherent auto-fluorescence, and therefore immune-fluorescence methods for characterization of surface proteins are not applicable [53]. The lack of a cytotoxic response indicates that no cytotoxic leachables were extracted from the materials during the 9 days 37 °C condition. Our observations on the in vitro cellular biocompatibility of PEEK-coated Nitinol correlate with previous studies where PEEK bulk material displayed excellent biocompatibility in mouse fibroblast L929 cells [54].

4. Discussion

While the inner bulk of a Nitinol alloy consists of its own nickel-titanium, the surface of as-received NiTi consists mainly of titanium oxide (TiO_2) and smaller amounts of nickel oxides (NiO and Ni_2O_3) with traces of metallic nickel and even traces of carbon for untreated surface substrates [12,16,37,51,55]. In solutions nickel may dissolve more easily than titanium because its oxides are not so stable. Therefore it is considered that the presence of a stable homogeneous titanium oxide layer at the surface can serve

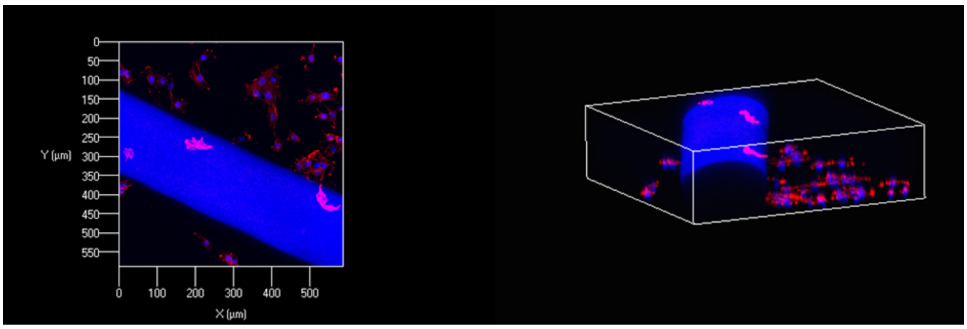

Fig. 8. Fluorescent confocal microscopy images of fibroblast cells having adhered to a PEEK-coated Nitinol wire after 24 h of incubation. Top view at the left, 3D reconstruction at the right. Nuclei fluorescence in blue, cytoplasm in red, and inherent auto-fluorescence of the PEEK also in blue. Note the healthy cells surrounding the wire on the surface of the culture well, and some crawling fibroblasts attached on the PEEK-coated wire. (For interpretation of the references to colour in this figure legend, the reader is referred to the web version of this article.)

as an effective barrier to nickel ion release. Moreover the decisive factor that determines resistance to corrosion has been shown to be the homogeneity of the oxide layer, rather than its thickness or component structure [9,12,51,55]. Thus the improvement is often attributed to the removal of the plastically deformed native oxide layer and its replacement by a newly grown, more uniform one. Our results using chemical etching followed by electropolishing for NiTi wires are now discussed in terms of the chemical reactions involved in the formation of the newly grown oxide layer at the surface (§ 4-1). Our method for obtaining an homogeneous stable oxide layer is of interest provided the latter is not disrupted by the subsequent PEEK layer deposition on top of it. This is discussed in § 4-2 together with the adherence strength and stability of this additional protective and biocompatible layer.

4.1. Reaction mechanisms involved in the NiTi surface preparation

Release of nickel ions takes its origin from the instability of the oxide layer (thickness varying within 2–20 nm) at the native NiTi alloy surface [12,16,37,51]. Whereas metal nickel dissolves according to the following equation (2):

$$Ni = Ni^{2+} + 2e^{-} \quad (2)$$

its main surface oxides NiO and Ni_2O_3 [16,37,55] are dissolved via a hydration step. Thus the detachment of a surface complex that resembles a fully hydrated metal in acidic solutions, $Ni(OH_2)_6{}^{2+}$, favors the nickel monoxide NiO dissolution [56]:

$$NiO + 2H^{+} \rightarrow Ni^{2+} + H_2O \quad (3)$$

whereas the dissolution mechanism of the black dinickel trioxide Ni_2O_3 involves the formation of oxyhydroxide NiOOH, followed by protonation and cleavage of metal-oxygen bond, and ultimate ion exchange, where intermediates such as $NiOOH_2{}^{+}$, $NiOH_2{}^{+}$, NiOH, and NiO^{+} may be encountered [57]. The equation of the overall process appears as:

$$2Ni_2O_3 + 8H^{+} \rightarrow 4Ni^{2+} + O_2 + 4H_2O \quad (4)$$

The leaching of nickel is favored in HF/HNO_3 solutions as revealed by the observed green color of the etching solution indicating the presence of Ni^{2+} ions.

Hydrofluoric acid that readily attacks TiO_2 reacts with Ti to form soluble titanium fluorides and hydrogen. Thus the Ti^{4+} ions migrate from the metal to the oxide/electrolyte interface and dissolve in the HF electrolyte forming complexes according to equation (5) [58]:

$$TiO_2 + 6F^{-} + 4H^{+} \rightarrow TiF_6{}^{2-} + 2H_2O \quad (5)$$

Incorporation of hydrogen in titanium can cause embrittlement of the surface layer and can lead to delayed fracture [59]. To avoid absorption of atomic hydrogen as a result of the acidic conditions created in pits and crevices during corrosion, a ratio of nitric acid to hydrofluoric acid of 10–1 was here used as it was shown to minimize the formation of free hydrogen [60].

Pickling is an effective method for removing the oxide film from the surface of metals. The mechanism of removal the oxide layer is as follows: the acid penetrates through cracks and pores on the surface underneath (Fig. 1), where the reaction with the metal takes place. As a result of this reaction there is some released hydrogen that accumulates inside. When the pressure reaches a certain amount the release of the gas induces collateral damage along the surface layers leading to a micron scale surface topography comprised of crater-like indentions with smooth walls (Fig. 2). This is why the time duration of pickling was found to be one of the critical parameters: it must be strictly controlled and should not be exceeded. As reported in §3-1 for wires about 3 cm long, 7 min appeared as an optimum duration for the process to allow sufficient time for the dissolution of the oxide layer.

Electropolishing of the alloy proceeds in two competing steps: anodic formation of the oxide layer and the chemical dissolution of this layer. In the initial stages of the anodization process field-assisted dissolution dominates chemical dissolution due to the relatively large electric field across the thin oxide layer [61]. In the first stage there proceeds oxidation of the surface, following the reaction (6):

$$M + H_2O = MO_2 + 4H^{+} + 4e^{-} \quad (6)$$

that is for the case of NiTi alloy the main reaction of the oxidation of its surface is as follows:

$$Ti + H_2O = TiO_2 + 4H^{+} + 4e^{-} \quad (6a)$$

Equation (6a) is indeed the main reaction as it is known that Ti has a higher affinity with oxygen (O^{2-}), when compared to Ni (the change in Gibbs free energy of formation $\Delta G(298\,K)$ is $-889\,kJ\,mol^{-1}$ for TiO_2, a value 4 times lower than to the $-211\,kJ\,mol^{-1}$ for NiO [62]). Therefore the formation of nickel oxides through equations (6b) and (6c):

$$Ni + H_2O = NiO + 2H^{+} + 2e^{-} \quad (6b)$$

$$2Ni + 3H_2O = Ni_2O_3 + 6H^{+} + 6e^{-} \quad (6c)$$

are not favored from a thermodynamic stand point [55,63]. Note also that since Ti bound in oxide is more stable than Ni bound, the release of Ni atoms in the aqueous solution leads to the presence of vacancies at the interface between the oxide scale and the NiTi substrate, which can promote the further reaction of oxygen with

Ti atoms. The second stage of the electropolishing process is the dissolution of the surface oxide into the aqueous solution through (7) for titanium oxide:

$$TiO_2 + 4H^+ \rightarrow Ti^{4+} + 2H_2O \quad (7)$$

and eventually through (3) and (4) for nickel oxides if formed anyway. The electropolishing process leads to a significant increase in the Ti/Ni atom concentration ratio on the surface [9,51,55,64] along with a reduced roughness as observed in Figs. 3 and 4. According to many reports of NiTi electropolishing at moderate temperatures, the oxide formed is composed mainly of TiO_2 with a slow formation and growth [16,55,64]. Note that the wire surface images obtained by SEM and AFM revealed the presence of some sparse white spots-points inclusion. Similar observations were reported in other investigations and interpreted as particles of titanium remaining in the oxide layer [38,65].

During the electropolishing process in perchloric acid mixed with acetic acid perchlorate anions migrate across the surface defects of oxide film formed on the ground surface and react with the substrate at the substrate/oxide interface. The reaction can be expressed by:

$$ClO_4^- + 8H^+ + 8e^- = Cl^- + 4H_2O \quad (8)$$

Reduction of perchlorate can process by direct contact with metal surface or by contact with partially oxidized metal ions released from the metal surface, which is generally promoted via pitting corrosion [66,67]. This mechanism is well illustrated when the anode potential or current density is too low: the resulting surface texture appears heterogeneous, composed of non attacked areas neighboring to other areas showing more or less hemispherical pits (Fig. 3a and b). Similarly at high potentials, the irregular fluctuations in the current density observed with time were an indication that film breakdown was taking place. Thus, as SEM shows (Fig. 3e) the surface exhibits irregular waviness reminiscent of a pitting-type attack indicating that over-polished NiTi wire leads to excessive removal of the surface. Another reason for degradation of the surface topography homogeneity and formation of microcracks in the oxide layer, as shown in Fig. 3d and e, is likely related to the spatial mismatch between the predominant phase TiO_2 in the scale which has a larger unit cell volume (0.062 nm^3 for rutile) than austenitic NiTi substrate (0.027 nm^3) [68]. All these aforementioned adverse effects explain why there were optimum conditions for anode potential, current density, and time, found in this work typically around the plateau value of 10 V anode potential and 0.3 A/cm^2 current density for a 3 min duration (Fig. 3c).

Chloride, which is the final reduction product of perchlorate, is released in the solution, but the reduction mechanism is complex and still under debate [69]. Indeed, direct reduction of perchlorate on the bare metal is thermodynamically infeasible due to the high anodic potential that is applied. This paradox has been noted for long [67], since the standard potential associated to equation (8) is 1.386 V smaller than the measured anode potential under polishing conditions. Different proposals have been suggested to explain the anomalous behavior observed during electrochemical dissolution of metals. It is possible that local potentials at the reaction sites are different and more negative than the apparent overall (measured) anode potential. It was also proposed that transient metal ions such as Ti(II) diffuse from the electrode surface and react with perchlorate in solution:

$$4Ti^{2+} + ClO_4^- \rightarrow 4TiO^{2+} + Cl^- \quad (9)$$

The intermediate Ti(II) is not common, but its existence has been shown by the presence of titanium halide ($Ti(X)_2$ where X = F, Cl, Br, or I) and titanium oxide TiO in solid phases [70]. In addition to the reaction (9) it was also suggested that electrochemically produced chlorine could oxidize the Ti(II):

$$Ti^{2+} + Cl_2 \rightarrow Ti^{4+} + 2Cl^- \quad (10)$$

Other possible mechanisms, such as an high ohmic potential drop across the oxide film, have also been proposed for the formation of the final product Ti(IV) [69]. Whatever is the actual explanation the proposed mechanism involving reduction of perchlorate ion by reaction with an anodically activated surface is consistent with many reports showing the presence of chloride ions in the vicinity of the metal surface [67,69]. Our observations are in agreement with the picture of a passive film breakdown initiated at discrete sites leading to dissolution by pitting. These sites are likely to correspond to preexisting flaws in the oxide layer that allow the perchlorate ions to penetrate and to react at the metal interface [67].

As a summary, chemical etching and electropolishing of Nitinol wires were shown to be efficient for the elimination of defective surface layers and surface oxidizing. Pickling appeared as a necessary step prior to any other one, as it removes the outermost surface layer of the alloy constituted of native rough and deformed oxides created during mechanical working. By setting optimized conditions, the electrochemical polishing lead to mirror-like surface finish. The smooth electropolished surface, as seen by SEM and AFM and which appears bright in the naked eye, results from a combination of the two following effects. Anodic leveling results from difference in the dissolution rate between peaks and valleys on the rough NiTi surface, while anodic brightening is associated with the suppression of the influence of the alloy microstructure on the dissolution rate. The quality of the surface oxide layer obtained in terms of homogeneity and uniformity is all the more beneficial and rewarding since it allows an additional protective layer to be deposited on top of it, while biocompatibility and stability under mechanical stress are achieved for the coated film, as we shall discuss it in the following section.

4.2. Stability of the PEEK coated film and biological implications

The previous section emphasized how successive cleaning, chemical etching, and electropolishing removed the native surface oxide layer and replaced it by a uniform and homogeneous one. The main functionality of this TiO_2 oxide layer is (i) to increase the stability of surface layers by protecting the bulk material from corrosion and (ii) to create a physical and chemical barrier against nickel oxidation and release from the NiTi wire. The subsequent coating with PEEK involved sintering at 400 °C of the dip-deposited thin film. This last step in the coating process could be a concern as different studies related some affects of thermal treatments on the oxide layer of NiTi alloys [9,12,17,37,64,71]. Not only heat treatments may modify the phase composition of the bulk, but they also may modify the Nitinol tendencies in formation of either Ti- or Ni-rich surface sub-layers [9,12,37,64,71]. Thus, for non pre-treated NiTi alloys it was reported that after oxidation in air at 300–500 °C for 30 min, a layer of TiO and metallic nickel is formed covered by a TiO_2 layer with $NiTiO_3$ [71] or with either Ni_2O_3 or $Ni(OH)_2$ [64]. However four arguments advocate for the absence of serious worries in the case of the NiTi wires processed as described in the previous section. The first remark is related to the smoothness and thickness of the oxide scale. These two characteristics are reported to undergo a dramatic change around 500 °C with a surface oxide becoming rough and thick at higher temperatures [71]. As the sintering of the PEEK deposited film is processed at 400 °C only an underlying thin and smooth oxide on the wire surface is likely to be maintained according to the observations reported for temperatures below that 500 °C threshold [71]: this is crucial because otherwise this oxide layer could be subject to cracks [9,12,51]. Sec-

ondly the sintering lasts 10 min only, and for such short durations it was also reported that the outward Ni diffusion and its accumulation in the external surface sub-layers are virtually nonexistent (see Fig. 6 and 9 of [71]). Thus the oxidation of the substrate surface is dominated by an inward growth of the oxide up to 400 °C [64]. As a result there should be no Ni-rich buried sublayers that otherwise could serve as a permanent Ni reservoir and a possible cause of toxicity. The third argument lies in the fact that this prevention is strengthened by preliminary chemical etching as it was shown to Ni deplete the external surfaces to a depth of up to ~90 nm after heat treatment [37]. Last but not least, as pointed by [17], electropolishing tends to create a surface almost free of defects and by the latter reduces the growth of thermal oxide growth and prevents enrichment in nickel in the outermost layers of the alloy. Indeed, Ni atoms in metallic state diffuse through defective TiO_x [72] and thus the uniform and homogeneous TiO_2 oxide layer as it was obtained by our process at the NiTi wire surface is protective. All these remarks harmonize for claiming that the thermal sintering of the PEEK film has not induced any detrimental effect and has not disrupted the protective surface oxide layer of the Nitinol wire. The absence of long and lasting Ni release, where a low nickel dissolution rate from PEEK-coated NiTi wires was measured in Hanks solution over long periods (see § 3–3), corroborates this conclusion.

In clinical applications, especially in orthopaedic implant conditions, localized mechanical stress or fretting may lead to surface layer damage or even removal of the passive film and can cause an increase in ion release or even a release of wear particles. The development of a biocompatible polymer coating, which remains cohesive and highly adherent to the Nitinol surface throughout its implantation (and deployment in the case of stents), is of great interest. It acts as a protective layer provided it resists cracking in pulsative oscillations and wear on contact points with other materials. The thin PEEK coating films obtained in different geometries of NiTi wires (see Fig. 5) are attractive due to their stability in solution and upon large mechanical deformation where no delamination was observed (§ 3-1). The scratch tests have given insights into the mechanisms that may disrupt the PEEK coating film (§ 3-2). This technique was used as it was considered simpler and more practical than conventional tests such as the peel test or pull off test, due to impracticalities of performing these tests on micro scale systems such as thin wires. In the same way scratch tests are techniques that solicit layers closer to the real applications. The applied stress which provokes cracking, partial or complete film delamination gives an idea of the adhesion strength, as we discuss it now.

For a scratched coating film the influence of the supporting substrate can be considered unimportant as long as the depth of penetration, h (defined as the displacement relative to the initial undeformed surface), is restricted to no more than 10% of the film thickness, t [73]. For PEEK films with $t = 12\,\mu m$, it appears that the scratch tests were actually driven in confinement ($h/t > 0.1$) for the larger part of their length (Fig. 7). As a consequence the plastic behavior into the layer will be increased in comparison with a bulk material. When the elastoplastic stress reaches the substrate interface, an elastic response will be generated into the substrate because the NiTi wire is superelastic. This elastic energy given to the substrate will be released after the completion of the scratch phase generating a residual stress between the coated layer and the substrate. Therefore the strain level for cracking generation and propagation in the case of confined materials will be reached for lower values of penetration depth. As a consequence the surface features observed by SEM after the scratch test and the inferred parameters provide the mechanical signature and characterization of the covering. For very weak applied loads, only the spherical part of the sphero-conical indenter penetrates the film. As observed by the absence of any groove trace the indentation is shallow and the film behavior is purely elastic. This is a regime where the semi-crystalline nature of the PEEK film has no effective part in differentiation between mechanical properties of the composite material consisting of spherulites within an amorphous matrix. It looks that the dispersed spherulites do not restrict the motions, slippage of the polymer chains. The depth, h^*, at which the spherical tip meets the flat face of the cone is $h^* = R(1 - \sin\alpha) \approx 0.59\,\mu m$ (sphere radius $R = 2\,\mu m$; cone of semi-angle $\alpha = 45°$). This corresponds to a cross-section diameter $2a^* = 2R\cos\alpha \approx 2.83\,\mu m$ for the projected contact area. These values indicate that the visible groove trace (from x ≈260 μm to 1000 μm) was drawn over its entire length with the cone having penetrated into the film. For shallow scratch depths the induced microcracks, as revealed in Fig. 6b, result from strain gradient effects existing in the PEEK film only. As soon as the radius of the projected contact area becomes of the order of $3a^*$ the mean strain, ε, is governed by the cone angle: $\varepsilon = 0.2\,\cot\alpha$ [74]. This occurs at a depth of penetration $h = h^* + (a - a^*)\cot\alpha \approx 3.4\,\mu m$ for which the applied load is ≈22 mN. Since the mean strain $\varepsilon = 0.2$ remains constant beyond this threshold up to the end of the scratch, all the observed and reported plastic deformations as seen by SEM (Fig. 6) are the result of the confined material between the tip and the substrate. In this plastic regime for the PEEK film one can calculate a mean pressure as

$$P_m = \frac{F_n}{\frac{1}{2}\pi a^2} \tag{11}$$

since during the scratch the contact area has the geometry of half-a-disk of radius a [75]. The latter value can be inferred from the groove width, $2b$, measured from the set of SEM images recorded all along the groove track by taking $a \approx b$. Remarkably, the mean pressure remains constant to a plateau ≈2.2 GPa as soon as $F_n \geq 52$ mN. This shows that larger applied loads cannot induce more plasticity in the PEEK film beyond a certain threshold. Increasing the normal load allows the tip to penetrate more deeply into the film only. As a consequence of increased confinement fractures are induced through cohesive defects. Note that these cohesive defects appear (Fig. 6d) above the critical load $F_c \approx 40$ mN defined in §3-2 beyond which the tangential force starts to fluctuate (Fig. 7). Their density increases and their sizes become larger as the tip penetrates further while approaching the NiTi interface. Ultimately the cohesive defects have become so spatially spread (>6 μm) that they succeed to expose the NiTi substrate (Fig. 6f) despite the fact that the tip has not touched it yet (penetration depth ≈9.5 μm that is ≈2.5 μm from the interface).

As a conclusion it appears that our deposition process has succeeded the PEEK coating film to have extremely good adhesive properties on Nitinol wires. Scratches, even with large local applied mean pressure (2.2 GPa), are not able to delaminate the film. This result is remarkable as polymer damage by scratch would uncover a substrate material, create crevice conditions and thus aggravate corrosion. Here, disruption is not induced by failure of the adhesive strength at the PEEK/NiTi interface, but by cohesive defects of the PEEK material. The increase of the mean strain via the confinement induces microcracks and cohesive defects in the PEEK film. A further increase in the deformation creates larger fractures. When the cohesive defects attain a sufficient size the film/substrate interface is reached generating fractures at the interface. The baring of the support is ultimately implemented with exposed portions of the substrate. However, what is remarkable is that the interface has sufficient strength to transfer stresses and strains to the coated material when topographic changes of the Nitinol wire occur. Our results show that mechanical deformation of coated NiTi springs (Fig. 5) do not cause adhesion failures, despite large induced local plastic deformation. Thus the interface retains sufficient strength to transfer stresses and strains to the

coated material. This is very encouraging and augurs well pursuing in coating Nitinol in more complex geometries, as plastic deformations can reach up to 25% in high stress area (nodes), as evaluated by numerical simulation for stent expansion for instance [76].

The data in our study demonstrate that the coating of NiTi wires with a PEEK film has no deleterious effects on the cells used in the context of our assessment criteria. Together with the observed absence of long and lasting Ni release our process provide PEEK-coated Nitinol wires with biocompatibility properties. However, one can note that because PEEK is chemically inert, and due to its hydrophobic surface, neither allows protein absorption nor promotes cell adhesion to a great extent [1,77]. For this reason the primarily inert PEEK could be modified in regard to its surface characteristics so that the surface will enhance cell adhesion and bioactivity. Several avenues have been proposed; in particular recent advances have shown that PEEK can be converted into a material with a high bioactivity by using the plasma technique [78]. Such a route is currently examined for PEEK-coated NiTi wires.

5. Conclusion

Because of their appealing mechanical properties, NiTi alloys have gained in popularity in the biomedical field. However, the issue of nickel release in the physiological environment from Nitinol alloy is important because this element is frequently involved in hypersensitivity and toxic reactions. The low dissolution nickel rate in physiological solution together with biocompatibility in vitro as shown in our study, promote PEEK-coated NiTi alloys in long-term implants. This study has shown that improvement is due to the modification of surface characteristics. By encompassing all the spatial scales from the mesoscopic to the nanometric ones, both from the chemical and physical points of view, we insured the best homogeneous microstructure over the entire surface of the NiTi wire. Not only chemical etching followed by electropolishing creates a homogeneous and smooth surface oxide layer, but the PEEK coating film protects the surface further from other processing, such as mechanical wear, fretting, and scratches during implantation. It is suggested that the good corrosion properties and the related promising biological response may be ascribed to the presence of an homogeneous TiO_2-based surface layer on top of which the protective biocompatible PEEK coating film has been homogeneously deposited without disrupting it. With the ever-expanding use of polymer coatings in the biomedical industry, a strong adhesive strength between Nitinol and coatings is an important endeavor. Our results have demonstrated that thin PEEK films, which coat straight and helicoidal NiTi wires, do not delaminate in solutions and when subjected to a mechanical stress in continuous cycles of axial compression/stretching at 20% strain for 7 million cycles. However, a relative weakness in the cohesive properties of the highly adherent PEEK film to the Nitinol surface has been noted. Large pressures (>2 GPa) applied locally may fracture the PEEK film via induced cohesive defects that ultimately lead to exposure of the metal substrate. To overcome this failure carbon fibers and other fillers may be added to improve the wear resistance and strength of PEEK materials [1,4–6]. In addition, the bioactivity of the already biocompatible PEEK-coated NiTi wires could be enhanced by different techniques such as plasma treatment [1,78]. On the ground of the already obtained results that allowed long-term durability and integrity for the coating to be demonstrated in different geometries, we pursue along these two aforementioned routes. Indeed, the various properties of the polyetheretherketone family make these polymers good candidate materials for the construction of medical devices in many applications.

Acknowledgments

Christophe Contal, Damien Favier, Jean Iss, Nicole Levis are gratefully acknowledged for their technical help. The experiments were carried out with equipment belonging to the Microscopy platform and the Micro Nano Mechanics Platform that are both housed at Charles Sadron Institute, C.N.R.S., Strasbourg, France.

References

[1] Steven M. Kurtz (Ed.), PEEK Biomaterials Handbook, Elsevier Inc., U.S.A, 2012.
[2] D.F. Williams, A. McNamara, R.M. Turner, Potential of polyetheretherketone (PEEK) and carbon-fibre-reinforced PEEK in medical applications, J. Mater. Sci. Lett. 6 (1987) 189–190.
[3] K.B. Kwarteng, C. Stark, Carbon fiber reinforced PEEK (APC-2/AS-4) composites for orthopaedic implants, Sampe Q. 22 (1990) 10–14.
[4] A.J. Goldberg, C.J. Burstone, I. Hadjinikolaou, J. Jancar, Screening of matrices and fibers for reinforced thermoplastics intended for dental applications, J. Biomed. Mater. Res. 28 (1994) 167–173.
[5] S.M. Kurtz, J.N. Devine, PEEK biomaterials in trauma, orthopedic, and spinal implants, Biomaterials 28 (32) (2007) 4845–4867.
[6] I. Nakahara, M. Takao, S. Bandoh, N. Bertollo, W.R. Walsh, N. Sugano, Novel surface modifications of carbon fiber-reinforced polyetheretherketone hip stem in an ovine model, Artif. Organs 36 (1) (2012) 62–70.
[7] L. McD. Schetky, M.H. Wu, Issues in the further development of nitinol properties and processing for medical device applications, in: Sanjay Shrivastava (Ed.), Medical Device Materials: Proceedings from the Materials and Processes for Medical Devices Conference (2003) 271–276.
[8] L.S. Castleman, S.M. Motzkin, The biocompatibility of nitinol, in: D.F. Williams (Ed.), Biocompatibility of Clinical Implant Materials, CRC Press, Boca Raton, USA, 1981, pp. 1129–1154.
[9] S. Shabalovskaya, J. Van Humbeeck, Biocompatibility of shape memory alloys, in: T. Yoneyama, S. Miyazaki (Eds.), Shape Memory Alloys for Medical Applications, Woodhead Publishing Limited, Cambridge, UK, 2008.
[10] U. Blum, G. Voshage, J. Lammer, F. Beyersdorf, D. Tollner, G. Kretschmer, G. Spillner, P. Polterauer, G. Nagel, T. Holzenbein, Endoluminal stent-grafts for infrarenal abdominal aortic aneurysms, N. Engl. J. Med. 336 (1997) 13–20.
[11] S. Miyazaki, Medical and dental applications of shape memory alloys, in: K. Otsuka, C.M. Wayman (Eds.), Shape Memory Materials, Cambridge University Press, Cambridge, 1998, pp. 267–281.
[12] S. Shabalovskaya, J. Anderegg, J. Van Humbeeck, Critical overview of nitinol surfaces and their modifications for medical applications, Acta Biomater. 4 (2008) 447–467.
[13] S. Shabalovskaya, G. Rondelli, M. Rettenmayr, Nitinol surfaces for implantation, J. Mat. Eng. Perform. 18 (2009) 470–474.
[14] B. Thierry, M. Tabrizian, O. Savadogo, L.'H. Yahia, Effects of sterilization processes on NiTi alloy: surface characterization, J. Biomed. Mat. Res. 49 (1) (2000) 88–98.
[15] M. Arndt, A. Bruck, T. Scully, A. Jäger, C. Borauel, Nickel ion release from orthodontic NiTi wires under simulation of realistic in-situ conditions, J. Mater. Sci. 40 (2005) 3659–3667.
[16] D.J. Wever, A.G. Veldhuizen, J. de Vries, H.J. Busscher, D.R. Uges, J.R. van Horn, Electrochemical and surface characterization of a nickel-titanium alloy, Biomaterials 19 (1998) 761–769.
[17] B. Thierry, M. Tabrizian, C. Trepanier, O. Savadogo, L.'H. Yahia, Effect of surface treatment and sterilization processes on the corrosion behavior of NiTi shape memory alloy, J. Biomed. Mat. Res. 51 (2000) 685–693.
[18] S. Shabalovskaya, G. Rondelli, J. Anderegg, B. Simpson, S. Budko, Effect of chemical etching and aging in boiling water on the corrosion resistance of nitinol wires with black oxide resulting from manufacturing process, J. Biomed. Mater. Res. B Appl. Biomater. 66 (1) (2003) 331–340.
[19] M. Es-Souni, M. Es-Souni, H. Fischer-Brandies, Assessing the biocompatibility of NiTi shape memory alloys used for medical applications, Anal. Bioanal. Chem. 381 (3) (2005) 557–567.
[20] K. Yokoyama, K. Hamada, K. Moriyama, K. Asaoka, Degradation and fracture of NiTi superelastic wire in an oral cavity, Biomaterials 22 (16) (2001) 2257–2262.
[21] R. Guidoin, Y. Marois, Y. Douville, M.W. King, M. Castonguay, A. Traoreí, M. Formichi, L.E. Staxrud, L. Norgren, P. Bergeron, J.-P. Becquemin, J.M. Egana, P.L. Harris, First-generation aortic endografts: analysis of explanted Stentor devices from the EUROSTAR Registry, J. Endovasc. Ther. 7 (2) (2000) 105–122.
[22] M.M. Mazumder, S. De, S. Trigwell, N. Ali, M.K. Mazumder, J. Mehta, Corrosion resistance of polyurethane-coated nitinol cardiovascular stents, J. Biomater. Sci. Polym. Ed. 14 (2003) 1351–1362.
[23] N. Moritz, E. Vedel, H. Ylänen, M. Jokinen, M. Hupa, A. Yli-Urpo, Characterisation of bioactive glass coatings on titanium substrates produced using a CO_2 laser, J. Mater. Sci. Mater. Med. 15 (2004) 787–794.
[24] D. Krause, B. Thomas, C. Leinenbach, D. Eifler, E.J. Minay, A.R. Boccaccini, The electrophoretic deposition of Bioglass® particles on stainless steel and nitinol substrates, Surf. Coat. Technol. 200 (2006) 4835–4845.
[25] G. Tepe, J. Schmehl, H.P. Wendel, S. Schaffner, S. Heller, M. Gianotti, C.D. Claussen, S.H. Duda, Reduced thrombogenicity of nitinol stents—In vitro

evaluation of different surface modifications and coatings, Biomaterials 27 (2006) 643–650.
[26] A.R. Boccaccini, C. Peters, J.A. Roether, D. Eifler, S.K. Misra, E.J. Minay, Electrophoretic deposition of polyetheretherketone (PEEK) and PEEK/Bioglass® coatings on NiTi shape memory alloy wires, J. Mater. Sci. 41 (2006) 8152–8159.
[27] M. Burke, B. Clarke, Y. Rochev, A. Gorelov, W. Carroll, Estimation of the strength of adhesion between a thermoresponsive polymer coating and Nitinol wire, J. Mater. Sci.: Mater. Med. 19 (2008) 1971–1979.
[28] A.R. Boccaccini, S. Keim, R. Ma, Y. Li, I. Zhitomirsky, Electrophoretic deposition of biomaterials, J. R. Soc. Interface 7 (Suppl 5) (2010) S581–S613.
[29] J.X. Zhang, R.F. Guan, X.P. Zhang, Synthesis and characterization of sol-gel hydroxyapatite coatings deposited on porous NiTi alloys, J. Alloy Compounds 509 (2011) 4643–4648.
[30] F.H. Silver, Biomaterials Medical Devices and Tissue Engineering: an Integrated Approach, Chapman and Hall, London, 1994.
[31] D. Brunette, P. Tengvall, M. Textor, P. Thomsen, Titanium in Medicine, Springer, Berlin, 2001.
[32] Surface Engineering of Light Alloys: Aluminium, Magnesium and Titanium Alloys, Woodhead Publishing Limited, Hanshan Dong, 2010.
[33] S.H. Hitchcock, N.T. Carroll, M.G. Nicholas, Some effects of substrate roughness on wettability, J. Mater. Sci. 16 (1981) 714–732.
[34] A.W. Momber, in: A. Momber (Ed.), Blast Cleaning Technology, Springer, Verlag, Berlin Heidelberg, 2008.
[35] P. Kékicheff, M. Clauzel, Patent EP 09730734.2, US 12/937, 201, JP 2011503460.
[36] S. Shabalovskaya, J. Anderegg, Surface spectroscopic characterization of TiNi alloys for implants, J. Vac. Sci. Technol. A13 (5) (1995) 2624–2632.
[37] S. Shabalovskaya, J. Anderegg, F. Laab, P.A. Thiel, G. Rondelli, Surface conditions of nitinol wires, tubing, and As-Cast alloys. the effect of chemical etching aging in boiling water, and heat treatment, J. Biomed. Mater. Res. B Appl. Biomater. 65 (1) (2003) 193–203.
[38] H. Zhao, J. van Humbeeck, I. de Scheerder, Surface conditioning of nickel-titanium alloy stents for improving biocompatibility, Surf. Eng. 17 (2001) 451–458.
[39] M. Nishida, C.M. Wayman, T. Honma, Precipitation processes in near-equiatomic TiNi shape memory alloys, Metall. Trans. A 17A (1986) 1505–1515.
[40] M. Pohl, C. Heßing, J. Frenzel, Electrolytic processing of NiTI shape memory alloys, Mater. Sci. Engineer. A378 (2004) 191–199.
[41] S. Shabalovskaya, G. Rondelli, J. Anderegg, J.P. Xiong, M. Wu, Comparative corrosion performance of black oxide, sandblasted, and fine-Drawn nitinol wires in potentiodynamic and potentiostatic tests: effects of chemical etching and electropolishing, J. Biomed. Mater. Res. B Appl. Biomater. 69 (2) (2004) 223–231.
[42] L.D. Landau, B. Levich, Dragging of a liquid by a moving plate, Acta Physicochim. USSR 17 (1942) 42–54.
[43] B.V. Derjaguin, On the thickness of the liquid film adhering to the walls of a vessel after emptying, Acta Physicochim. USSR 20 (1943) 349–352.
[44] D.A. White, J.A. Tallmadge, A theory of withdrawal of cylinders from liquid baths, A.I.Ch.E. J 12 (1966) 333–339.
[45] D. Quéré, Fluid coating on a fiber, Annu. Rev. Fluid Mech. 31 (1) (1999) 347–384.
[46] S. Kumar, D.P. Anderson, W.W. Adams, Crystallization and morphology of poly(aryl-ether-ether-ketone), Polymer 27 (5) (1986) 329–336.
[47] D.J. Blundell, B.N. Osborn, The morphology of poly(aryl-ether-ether-ketone), Polymer 24 (1983) 953–958.
[48] A.A. Volinsky, N.R. Moody, W.W. Gerberich, Interfacial toughness measurements for thin films on substrates, Acta Mater. 50 (2002) 441–466.
[49] V. Le Houérou, C. Robert, C. Gauthier, R. Schirrer, Mechanisms of blistering and chipping of a scratch-resistant coating, Wear 265 (2008) 507–515.
[50] B.G. Pound, Corrosion behavior of metallic materials in biomedical applications. I. Ti and its alloys, Corros. Rev. 32 (1-2) (2014) 1–20.
[51] S.A. Shabalovskaya, H. Tian, J.W. Anderegg, D.U. Schryvers, W.U. Carroll, J. Van Humbeeck, The influence of surface oxides on the distribution and release of nickel from Nitinol wires, Biomaterials 30 (2009) 468–477.
[52] EU-RAR (EU Risk Assessment Report), Nickel and nickel compounds, Danish Environmental Protection Agency, Copenhaguen, 2008.
[53] A. Hunter, C.W. Archer, P.S. Walker, G.W. Blunn, Attachment and proliferation of osteoblasts and fibroblasts on biomaterials for orthopaedic use, Biomaterials 16 (1995) 287–295.
[54] L.M. Wenz, K. Merritt, S.A. Brown, A. Moet, In vitro biocompatibility of polyetheretherketone and polysulfone composites, J. Biomed. Mater. Res. 24 (1990) 207–215.
[55] C. Trépanier, M. Tabrizian, L.'H. Yahia, L. Bilodeau, D.L. Piron, Effect of modification of oxide layer on NiTi stent corrosion resistance, J. Biomed. Mater. Res. 43 (1998) 433–440.
[56] C. Ludwig, W.H. Casey, On the mechanisms of dissolution of bunsenite [NiO(s)] and other simple oxide minerals, J. Colloid Interface Sci. 178 (1996) 176–185.
[57] N.M. Pichugina, A.M. Kutepov, I.G. Gorichev, A.D. Izotov, B.E. Zaitsev, Dissolution kinetics of Nickel(II) and Nickel(III) oxides in acid media, Theor. Found. Chem. Eng. 36 (5) (2002) 485–494.
[58] W. Simka, M. Kaczmarek, A. Baron-Wiecheć, G. Nawrat, J. Marciniak, J. Zak, Electropolishing and passivation of NiTi shape memory alloy, Electrochim. Acta 55 (2010) 2437–2441.
[59] K. Yokoyama, K. Kaneko, K. Moriyama, K. Asaoka, J. Sakai, M. Nagumo, Delayed fracture of Ni-Ti superelastic alloys in acidic and neutral fluoride solutions, J. Biomed. Mater. Res. 69A (2004) 105–113.
[60] American Society for Testing and Materials, ASTM standard B600, Annual Book of ASTM Standard, vol. 2.04, American Society for Testing and Materials Philadelphia, PA, 1997, p.6.
[61] G.E. Thompson, Porous anodic alumina: fabrication characterization and applications, Thin Solid Films 297 (1997) 192–201.
[62] D. Wagman, W. Evans, V. Parker, R. Schumm, I. Halow, S. Bailey, The NBS tables of chemical thermodynamic properties, J. Phys. Chem. Ref. Data 11 (Suppl. (2)) (1982).
[63] S.A. Shabalovskaya, G.C. Rondelli, A.L. Undisz, J.W. Anderegg, T.D. Burleigh, M.E. Rettenmayr, The electrochemical characteristics of native Nitinol surfaces, Biomaterials 30 (2009) 3662–3671.
[64] D.A. Armitage, D.M. Grant, Characterization of surface-modified nickel titanium alloys, Mater. Sci. Eng. A349 (2003) 89–97.
[65] H. Zhao, J. van Humbeeck, I. de Scheerder, Surface conditioning of NiTi and Ta stents, Prog. Biomed. Res. 6 (2001) 439–448.
[66] J.B. Mathieu, H.J. Mathieu, D. Landolt, Electropolishing of titanium in perchloric acid-acetic acid solution. I. Auger electron spectroscopy study of anodic film, J. Electrochem. Soc. 125 (7) (1978) 1039–1043.
[67] J.B. Mathieu, D. Landolt, Electropolishing of titanium in perchloric acid-acetic acid solution. II. Polarization behavior and stoichiometry, J. Electrochem. Soc. 125 (7) (1978) 1044–1049.
[68] S.M. Green, D.M. Grant, J.V. Wood, XPS characterisation of surface modified Ni-Ti shape memory alloy, Mater. Sci. Eng. A 224 (1-2) (1997) 21–26.
[69] C. Lee, B. Batchelor, S.H. Park, D.S. Han, A. Abdel-Wahab, T.A. Kramer, Reduction of perchlorate using zero-valent titanium (ZVT) anode: reaction mechanism, Adv. Environ. Res. 1 (1) (2012) 37–55.
[70] U. Kölle, P. Kölle, Aqueous chemistry of titanium(II) species, Angew. Chem. Int. Edit. 42 (37) (2003) 4540–4542.
[71] G.S. Firstov, R.G. Vitchev, H. Kumar, B. Blanpain, J. Van Humbeeck, Surface oxidation of NiTi shape memory alloy, Biomaterials 23 (2002) 4863–4871.
[72] J.P. Espinós, A. Fernández, A.R. González-Elipe, Oxidation and diffusion processes in nickel-titanium oxide systems, Surface Sci. 295 (1993) 402–410.
[73] A.C. Fischer-Cripps, Nanoindentation, 3rd edition, Springer, N.Y, 2001.
[74] K.L. Johnson, Contact Mechanics, University Press, Cambridge, 1985.
[75] C. Gauthier, S. Lafaye, R. Schirrer, Elastic recovery of a scratch in a polymeric surface: experiments and analysis, Tribol. Int. 34 (2001) 469–479.
[76] F. Migliavacca, L. Petrini, M. Colombo, V. Montanari, I. Quagliana, F. Auricchio, G. Dubini, A predictive study of the mechanical behaviour of coronary stents by computer modelling, Med. Eng. Phys. 27 (2005) 13–18.
[77] O. Noiset, Y.J. Schneider, J. Marchand-Brynaert, Fibronectin adsorption or/and covalent grafting on chemically modified PEEK film surfaces, J. Biomater. Sci. Polym. Ed. 10 (1999) 657–677.
[78] D. Briem, S. Strametz, K. Schröder, N.M. Meenen, W. Lehmann, W. Linhart, A. Ohl, J.M. Rueger, Response of primary fibroblasts and osteoblasts to plasma treated polyetheretherketone (PEEK) surfaces, J. Mater. Sci.: Mater. Med. 16 (2005) 671–677.